

BIROn - Birkbeck Institutional Research Online

Kneller, B. and Roberts, Gerald P. and Grindrod, Peter (2019) Correlation between graben orientation, channel direction change and tectonic loading: The Elysium Province, Mars. *Journal of Geophysical Research: Planets* 124 (3), pp. 652-680. ISSN 2169-9097.

Downloaded from: <https://eprints.bbk.ac.uk/id/eprint/26480/>

Usage Guidelines:

Please refer to usage guidelines at <https://eprints.bbk.ac.uk/policies.html>
contact lib-eprints@bbk.ac.uk.

or alternatively

Correlation between graben orientation, channel direction change and tectonic loading: The Elysium Province, Mars.

B.D.Kneller¹, G.P.Roberts², and P.M. Grindrod³

¹ Department of Earth and Planetary Sciences, University of London, London, UK.

² Department of Earth and Planetary Sciences, University of London, London, UK.

³ Department of Earth Sciences, Natural History Museum, London. UK

Corresponding author: Brian Kneller (kknel01@mail.bbk.ac.uk)

Key Points:

- Graben are systematically arranged around sources of volcanically generated stress, lithospheric loading or regional stress;
- A common sequence of region wide stress events that correlate with graben direction and orientation of channels of differing morphology;
- A development sequence for the NW Elysium Province is proposed using graben orientation and channel direction analysis.

Abstract

We have investigated the links between regional stress fields, the volcanic centers, rifts, graben and channels in the NW region of the Elysium Province (Fig 1(a) and Fig 1(b)) to determine whether the sequence of stress events occurring during province development can be derived from the morphologies of these features; and thus provide a sequence of development events, which is independent of surface dating techniques. Rift and graben geomorphology was mapped and the neighboring relationships and orientation of individual graben were assessed to determine any spatial clustering or preferred orientation with regional or surface features capable of creating lithospheric flexure or tectonic stress within the study area. Crosscutting analysis determined a time ordered sequence of graben formation and these were related to volcanic centers or regional sources of stress. In addition, mapping showed that different channels share sections with similar shape and orientation, prompting our study of whether these channels, in tandem with the graben, were tectonically influenced during their development. The channel central axes were mapped and compared to identify common sequences of channel direction change. The time sequence of channel direction changes and the time ordered sequence of graben development were then compared. We have demonstrated a correlation between rift and graben direction with channel orientation suggesting a regional stress control from evolving volcanic centers. Overall we derive, for

the first time, the temporal pattern of tectonic, volcanic and channel evolution for the northwestern region of this major magmatic province on Mars.

Plain Language Summary

The northwest region of the Elysium Volcanic Province includes volcanoes, large outflow channels and narrow straight valleys called graben. We noticed that some outflow channel shapes matched, and nearly all graben were arranged in lines, curves or clusters. Analyzing these arrangements we identified a sequence of geological events that could have created the Province. With mapping and analysis we have shown the outflow channel directions, and the location and direction of graben, have been controlled by the same tectonic forces. As events changed in time the force direction also changed, allowing us to identify probable events, for example volcano growth. We suggest the Province elevation increased as magma rose from the Martian interior; then the Hecates Tholus volcano increased in size; followed by the growth of Elysium Mons, the largest volcano in the Province. We suggest some lava erupted by Elysium Mons flowed away in subsurface channels called dikes to the surrounding Province, creating graben similar to some features seen in the northern Canadian Shield. These results are important since this is the first time the Province growth events have been measured in this way, and the results are more accurate than some earlier attempts to predict this history.

1 Introduction

Significant portions of the Martian surface are dominated by the presence of large volcanic centers containing numerous volcanic edifices, associated rift zones, graben, and channels; yet the relative timing and details of their development remain elusive. Some progress has been made using stratigraphic superposition, cross cutting relationships, and surface dating techniques, which have proved to be inconsistent and uncertain in their outcomes. This study, using a different approach, seeks to provide greater certainty in the understanding of the sequence of volcanic center development by mapping the directions and intersections of associated rift zones, graben, and channels and analyzing these data.

One link between the volcanic centers, rifts and channels may be the stress field associated with the volcanic edifices. Detailed pioneering work on the stress field was carried out by Hall et al., (1986) who modeled the lithospheric flexural response to volcanic loading (Fig. 1c) as thin elastic shell flexure overlying an inviscid fluid interior. Hall et al. (1986) adjusted the possible lithospheric loads to create a stress field that could account for the locations and relative orientations of surface tectonic features. This model did not account for volcanically created stress or provide a time ordered sequence of events. Other workers considered volcanically created stress distributions in particular Grosfils (2007) using the finite element method (FEM) of stress analysis. The Grosfils (2007) model, and later models by Hurwitz et al. (2009), Galgana et al. (2011), Bistacchi (2012) and Galgana et al. (2013) considered various scenarios including magma chamber shape, chamber overpressure, volcano development stage, structural features and variances in volcanic behavior to predict both

the lithospheric flexure and fracture orientations. McGuire (1989) and Nakamura (1977) provide an understanding of the regional interplay of stress variations created by regional tectonic events and volcanic processes occurring during province development.

Here we ask whether it is possible to gain insights into how stress has changed through time in the region by examining crosscutting relationships between graben and by studying the time evolution of the channels. In particular, we ask whether rifts and channels are aligned, and if they are preferentially aligned with the volcanoes or other identifiable stress sources.

Our initial observations led us to note four main features.

(1) From a visual comparison within the area, some channels appear to have sections that are similar in shape and orientation to one another, possibly suggesting synchronous formation, and we ask whether these features can be related to shared tectonic influences. For example, Figure 1a shows the similarity in the axial orientation of channels that we name 1 and 2. Starting from their mouths; considering channel 2 direction indicators, which first indicate a channel direction of ESE, then turning to ENE continuing to SE, then SES, then SE, then SES and finally pointing towards ENE. Channel 1 makes the same directional changes, and often within similar shaped channel sections. This similarity in orientation is striking and somewhat unusual as it suggests that orientation changes are not simply meander development, but instead relate to an external cause that is shared between these channels. We further noted that many channel direction indicators do not link the shortest path between successive contours and therefore do not flow along the direction of maximum slope.

(2) Visual inspection also reveals crosscutting relationships between rifts or graben of different orientation, and again we ask whether these features can be related to tectonic influences and whether there is a time order in these relationships.

(3) The initial observations of graben crosscutting showed a sequence of directional change possibly similar to the common time sequence implied by the channels. For example, most graben axes orientated in a NW to SE direction are only crosscut by those orientated towards Hecates Tholus.

(4) An initial analysis of rift and graben direction shows that graben with similar azimuth are clustered and often pointing towards a surface feature (Fig 2).

Detailed investigations of these points could increase the understanding of past regional tectonic activity, and the order of volcanic center development, which is the overarching aim of this paper.

1.1 Study Approach

We selected the Elysium volcanic province for the study, as it includes channel features (Fig 1a), the volcanoes of Elysium Mons (EM), and the two flank volcanoes, Hecates Tholus to the north and Albor Tholus to the south

. The channels and graben features investigated are located on the NW flank of the Elysium Rise between Utopia Planitia, which borders the northern and western flank of the Elysium Rise, and the Elysium Mons summit caldera.

The study was organized as follows. First, a sample of rift and graben orientations were measured and the resulting probability density function was used to substantiate our observation that spatially clustered graben pointed in similar directions often at a surface features (Fig 2). All rift graben orientations within the study area were then measured producing a multimodal distribution containing a mixture of distributions and variables of location and azimuth. From these data multivariate Gaussian distributions were extracted. For each distribution the mean was used to identify a possible source of dilatational stress (e.g. a volcanic center), and if the distribution mean azimuth pointed towards one, then the distribution members and the source of stress were color coded to indicate this relationship and to aid visualization. The graben crosscutting analysis used this information to determine a time order for changes in regional stress direction. Secondly, changes in orientation along the length of channels were quantified by mapping. Then the technique of ‘dynamic time warping’ (Giorgino, 2009) was used to search for correlations between channels to determine possible synchronous long axis changes in orientation during their development. Dynamic time warping compared channels by aligning matching sections on a common axis; thus making channel propagation rates a non-critical factor especially in the comparison of channels of dissimilar lengths. These shared channel long axis variation signatures were then compared with the time ordered regional stress direction change derived from the graben cross cutting analysis to see if regional stress could have influenced channel direction during development. Once established this time ordered sequence of stress direction change was used to identify the progression of tectonic processes identified by the models cited in this paper.

2 Study Area Geology

2.1 Geomorphology

Eight channels are major features in the study area on the Elysium Rise (Fig 1a) and were included in this study. With the exception of the channels we name 3, 4 and 5, the channel major axes are aligned radially with the Elysium Mons summit caldera (Fig 1a). Channels 2 and 8 are on the lower, steeper slopes of the Elysium Rise and differ markedly in their morphology. Channel 2 could be identified as theatre headed in its lower regions, but the tapered head is non-characteristic, and Channel 8 is rille-like. Channel 2 has flow parallel ridges at a similar elevation (-1000m) to the head of Channel 8. Channels 1, 3, 4, 5 and 6 have developed in a region of lower gradient on the crest of the Elysium Rise. Channels 4 and 5 axes orientate to the NE flanks of Elysium Mons. Channels 3, 4 and 5 appear as raised tributaries and connect to Channel 1. The upper sections of Channel 6, though smaller, has similarities with Channel 1. There are other similarities specific to Channels 1 and 2; for example, each has a flow parallel channel to the south of the main channel in the lower reaches and flow parallel channel to the north of the main channel towards both channel heads, refer to S2 for enlarged images. The outfall from these channels feed into the Utopia Planitia Basin in the NW (Thomson et al., 2001).

The distribution of graben clusters vary across the area (Fig 1b), and referring to the center of the NW and SE quadrants, several bands of graben can be seen linearly aligned in a NW to SE direction. Cross cutting these in the NW quadrant are bands of graben tangential to Hecates Tholus . The graben clusters around Elysium Mons in the NW quadrant are concentrically arranged at varying distances from the edifice, which is similar to the cluster alignments in the NE, SE and SW quadrants. In addition there is a concentric cluster proximal to Albor Tholus, with further clusters to the N and the SE of this edifice. The complex graben distribution in the SW quadrant has the vestiges of a linear graben alignment similar to those seen in SE quadrant, and there are other clusters and linear graben alignments that require further investigation; these however the analysis of these are not within the scope of this study.

Finally, many surface features have been created in a low gradient region, which has under gone uplift, and these are cross cut or partially covered by a range of sedimentary or volcanic surface deposits. The channels considered crosscut the major flank flows though there is evidence of more recent surface deposits and some later minor surface flows within them.

2.2 Stratigraphy

There are three major stratigraphic units within the study area (Tanaka et al., 2014) Fig 1(d). The main edifice, Elysium Mons and the flank cones of Albor Tholus and Hecates Tholus are Hesperian volcanic edifice units (Hve) comprising lobate flows up to tens of meters thick and tens to hundreds of kilometers across. These units are surrounded by younger Amazonian/Hesperian volcanic units (AHv), with flows tens of meters thick, and hundreds of kilometers long resulting in an accumulated thickness of several kilometers. Both AHv and Hve surround a late Hesperian volcanic field (IHvf) comprising smaller lobate flows tens kilometers long and several meters thick. This flow is bounded in the north by the southern wall of Channel 1.

2.3 Volcanic History

The history of Mars volcanism has been the subject of many studies, and in more recent papers the focus has tended towards caldera age dating to identify the most recent eruption events. Greeley and Spudis (1981) first described the volcanic history based on observations of stratigraphic superposition and cross cutting. There followed various crater-dating studies that produced significant discrepancies between crater model ages. These were due to differences in data set spatial resolution; differing data fitting methods and chronology functions; differing choice of counting area; misidentification of surface features; and neglect of the regional geology (Platz and Michael, 2011; Hartmann, 2005; Hartmann and Neukum, 2001). Werner (2009) examined several volcanic centers including the Elysium Province and Tharsis Montes. A coherent data set was produced based on a standardized crater dating method, the use of CTX high-resolution images for measurement and analyses by a single observer. The data produced included an age estimate for the main edifice erection by dating flank deposits, and estimates of the most recent volcanic activities from caldera floor analyses. Werner (2009) concluded the main edifice emplacement dates for the following volcanoes are; Elysium Mons 3.7 Ga, Albor Tholus before 3.4 Ga, Hecates Tholus 3.5 Ga and Tharsis Montes complex 3.55 Ga. Activity continued with all

volcanoes declining at different rates from approximately 1 Ga. Robbins et al. (2011) analyzed 20 large volcano caldera including the Tharsis Montes complex, but using smaller caldera sample areas than Werner (2009). The sampling areas were determined using geomorphological features and surface cover to subdivide the caldera floors. Robbins et al. (2011) used a dating methodology different to Werner (2009) and discrepancies were found, some due to caldera area subdivision. Robbins et al. (2011) provided a range of dates that are dependent on caldera activity only and did not consider flank activity. Platz and Michael (2011) however provided an eruption history specifically of the Elysium Province using selected areas on the flanks, and in the caldera and concluded the earliest activity was 3.9 Ga with a major activity peak 2.2 Ga when the majority of material was erupted over a 200 Ma interval. The youngest flood lava found to-date, in Athabasca Valles, was dated as 5Ma +/- 2Ma (Jaeger et al., 2010). From the above, the variation in assumptions, measurement methods, data sets and loosely constrained timescales, often result in overlapping time ranges, making the sequence of volcanic activity on the Elysium Province difficult to establish.

Fluvial erosion was most active from late Noachian through to early Amazonian (Carr and Head, 2010), (Hynek et al., 2005) and a variety of flow regimes have been considered for this this region. The major fluvial activity is considered to have taken place in the Noachian.

3 Background

This section provides more detail on the bodies of understanding used within this study, in particular works relating to lithospheric loading, changes in edifice stress due to volcanic process, graben and tension fractures, and finally, the effects of surface erosion within the context of this paper.

3.1 Lithospheric Modelling

Initially Janle and Ropers (1983) calculated lithospheric loading from regional topography and compared these to Mars Global Surveyor (MGS) line of sight (LOS) Doppler gravity variations to determine levels of isostatic compensation. Later Comer et al. (1985) modeled lithospheric flexure using a single conic load model centered on Elysium Mons and estimated the lithospheric effective elastic thickness ($T_e = 54\text{km}$) inferred from the observed concentric graben positioning. Comer et al. (1985) argued concentric graben at a distance from an edifice were the result of lithospheric flexure. Hall et al. (1986) agreed with the value of T_e and the region of concentric flexure determined by Comer et al. (1985). The lithospheric model by Hall et al. (1986) identified more sources of stress than Comer et al. (1985) incorporating Tharsis isostatic stress and flexural loading (Banerdt et al., 1982), Elysium Planitia deposits, magma plume related uplift, and volcanic loading by Elysium Mons and Hecates Tholus; Albor Tholus mass was considered insignificant. Predictions of horizontal regional stress were calculated by modeling the lithosphere as a flexible shell on an inviscid fluid, and applying combinations of the above loads. Hall et al. (1986) concluded loading from Tharsis isostatic flexural stress, plume related Province uplift and the individual loads of Hecates Tholus and Elysium Mons provided the best fit with the regional tectonic features (Fig 1c). In more recent studies McKenzie et al. (2002) used Cartesian

domain admittance techniques with Viking 2 topography data and MGS LOS Doppler gravity data ($T_e = 27$ km). McGovern (2002) used spectral domain analysis with MGS LOS gravity and MOLA topography data ($T_e = 60$ to 90 km); while Belleguic et al. (2005) created a revised spectral model with similar data ($T_e = 54$ km). None of the recent authors produced maps of the Elysium Rise detailing the distributions of compressional and dilatational stresses within the study area with the exception for Hall et al. (1986), which we used; consequently any coherence between these other data and ours could not be demonstrated.

3.2 Volcanic Edifice Modelling

The current models of volcanic edifice stress distribution are summarized below and these have been applied to a variety of scenarios including generalized, terrestrial, Martian and Venusian environments. With the support of field, petrological and remote sensing analysis finite element (FEM) half space models have provided insight into the stress variations associated with volcanic activity including magma flow, magma chamber shape, size and location, edifice growth and lithospheric flexure. Grosfils (2007 and the references therein) summarize the analytic approaches to the data within the paper and compare them with an FEM model, which primarily considered the variation in magma chamber rupture with depth of burial. Hurwitz et al. (2009) expanded the model to include the impact of edifice growth on chamber rupture behavior and predicted the blocking of magma ascent and magma flow re-routing to radial flow on edifice mass increase. Galgana et al. (2011) incorporated the effects of lithospheric flexure into the model and Bistacchi extended the rheological behavior and demonstrated correlation between the model (Bistacchi, 2012) and the distribution of cone sheets and dikes in the Cullen Igneous Province. Most recently Galgana et al. (2013) modeled the effects of uplift on magma chamber rupture constraining the temporal and cyclic aspects of eruption and uplift and the conditions for inhibiting magma ascent and diversion to radial flow. These models account for the formation of radial and circumferential dikes, cone sheets, sills and lithospheric flexure depending on the scenario considered. No model exists for the Elysium Province consequently these models have been used in the arguments presented here.

3.3 Graben and Tension Fractures

There is a general consensus within the references quoted (including Golombek, 1989; MacKinnon and Tanaka, 1989; Ernst et al., 1995; Ernst et al., 2001; Wyricket et al., 2004; Pederson et al., 2010) that features considered here are the product of dilatational rupture, which is considered as the dominant process in graben, channel and rift formation on Mars. However it should be noted that graben can form with high levels of the principle maximum component of stress, σ_1 , acting vertically during up-thrust but this would not generally apply; with the possible exception of stress related features associated with regional uplift. The formation of graben by dilational stress, requiring intact rocks (MacKinnon and Tanaka, 1989), is well documented. Ferrill and Morris (2003) who summarize the environment by assigning the principle minimum component $\sigma_3 < 0$, σ_3 is greater than or equal to the tensile strength of the rock, and has a zero angle of shear between the fault surfaces. This stress vector acts parallel to the horizontal and in the case of a graben, is perpendicular to graben wall orientation. This vector, termed the graben azimuth, points in the general direction of the stress source.

There are several processes that influence graben formation and these include collapse features related to sub-surface dikes. Several researchers have considered the sensitivity of magmatically created near surface dikes and dike swarms to tectonic influence (Ernst et al., 1995). Generally, radial dikes can form proximal to a magma body indicating random dike propagation in response to individual pressurization events in a regionally homogeneous stress field (Pedersen et al., 2010). Further away from the magma source curved and linear, sub-parallel, near-surface dikes tend to propagate in a direction perpendicular to the direction of regional minimum horizontal compressive stress (Ernst et al., 2001); or the maximum horizontal tensile stress, σ_3 . Also, tension fractures can include basement faulting below the unconsolidated Martian upper crust producing inline surface subsidence features, e.g. crater pit chains and surface wedges (Wyricket al., 2004). In comparison, Golombek (1989) cites the simple graben as the most common surface feature with two inward facing symmetric normal faults and scarps of equal height; with a flat floor; where the absence of the latter is used to differentiate joints and tension fractures. Tension fractures occur in a variety of forms and within this paper the term graben is used to describe any form of tension fracture unless stated otherwise. In summary, graben or rifts can be created by a wide variety of sources from those originating at a regional level through to the local effects of edifice structural loadings.

3.4 Channel Erosion

The study area contains channels whose development on Mars are primarily attributed to water, water mediated material flow or lava, and this section identifies these possibilities.

Studies have considered fluvial erosional processes linked to channel development and these are now identified. Howard et al. (2005), considered the late Noachian / early Hesperian to be the apparent peak in fluvial activity caused by precipitation. Other types of erosional processes considered to be active in the study area occurring in the interval between the Late Noachian through into the Late Amazonian include syn-volcanic mega-lahars (Christiansen, 1989); Amazonian syn-volcanic fluvial and peri-glacial activity (Tanaka, 1992); lahar creation from effused groundwater (Russell & Head, 2003), and fluvial or ground water environments from Late Amazonian glaciers (Madeleine et al., 2009). The effused ground water from the Martian global aquifer within the study area is not available due to the elevation limit of less than -3000m, Clifford (1992). In the study area Carr and Clow (1981) suggested flow in these channels could have been created by processes other than fluvial, a view supported by Leverington (2011) who proposes lava as the principle erosive agent. The study area channels can be divided into arcuate rille-like and theatre headed channel morphologies, which are now discussed

Terrestrial theater-headed channels (Laity and Malin, 1985; Laity et al., 1990; Lamb et al., 2006; Schultz et al., 2007) are fluvial in origin, and the direction and parallelism of their walls are considered to be controlled by faults or regional jointing.. These channels can develop from ephemeral surface water flow down the line of maximum slope creating narrow gullies which later widen by mass wasting, possibly ground water sapping

(Lamb et al., 2006). Alternatively channels can develop headward due to ground water sapping only by aquifer water erosion in the canyon head walls without surface water flow (Laity and Malin, 1985). In both cases faults and jointing can control the channel flow direction. If the channels are controlled by fault, fracture or rift orientations, one direction of control is parallel to the channel axes perpendicular to the direction of principle direction of maximum tensile stress, σ_3 . Alternatively, the direction of σ_3 can act parallel with the channel axis producing faults and jointing perpendicular to the channel axis at the head wall controlling the direction of headward erosion (Lamb et al, 2014).

Next we will consider arcuate and linear rille-like channels. We refer to channels similar to Channel 8 (Fig 1a) as arcuate rille-like because their characteristics include consistently straight or arcuate parallel striking walls bounded by steep inward dipping slopes; their directions typically ignore topographic obstructions; they cut across highland terrains, and they exhibit little change in propagation direction, McGill (1971). Both arcuate and linear rilles are considered to be linear arrays of graben created in tensional fields associated within various stress related contexts (Head and Wilson, 1993). Basin formation and subsequent lithospheric loading by basin fill create rilles e.g. McGill (1971); Solomon (1980) or localized dilatational stress fields can create arcuate rille-like features by near surface dike emplacement (Head and Wilson, 1993). The propagation direction of arcuate and linear rille development is open for consideration as this is dependent on preexisting or contemporaneous tectonically generated pathways. The creation direction of these paths on volcanic slopes depends on local edifice stress distribution, regional and gravitational stress (McGuire, 1989). Volcanic processes determine flank eruptions, which can be sourced from the volcano central conduit via dikes either vertically or horizontally orientated for more distal eruptions. Alternatively flank eruptions can occur from dikes fed vertically from below the edifice from a less fractionated and deeper magma sources (Geshi, 2008). This behavior has been observed on Etna (Acocella, 2003) in the 2001 eruption. In this instance main conduit magma was supplied to a series of downslope propagating fissures; whilst another form of dike referred to as an “eccentric dike”, formed contemporaneously in the same area erupting less differentiated magma (Bonoforte, 2009) however these fissures propagated up slope. Acocella, (2003) noted Etna flank extensional instability due to regional influences as a possible influence on the development of these features, and this is not dissimilar to the NW flanks of EM which lack buttressing due to the proximity of the Utopia Planitia basin (Thomson et al., 2001).

Rille-like features and theatre headed channels can share common controls for direction development but conventionally they differ in their development direction. The direction of channel development is important in our analysis but the type of flow is less so. The unavailability of sufficient volumes of subsurface or surface water at the channels elevations considered makes sustained fluvial events capable of producing the channels unlikely (Carr et al., 1981). However, ephemeral supplies of water from glacial deposits, snow and eruptive events make it possible for water-mediated flows or aquifer born seepages to flow down the line of maximum slope if unimpeded. Likewise surface flowing lava could behave in a similar manner creating sinuous channels referred to as sinuous rilles in a Lunar context. Arcuate rilles are a special case as they are not necessarily generated by flow as it is considered the direction of these channels is controlled by pre-existing or contemporaneous tectonic events. Due to this, the direction of their development is not necessarily down the line of maximum slope but is determined by the local stress direction, and the feature propagation can be upslope.

4 Methods

This section describes the key data required to support the study and how this was derived from the collected data and identifying the methods used in the analysis. The emphasis has been to maximize accuracy, repeatability and minimize observer bias. The application software and workflows producing these data are described below.

4.1 Applications and Software

4.1.1 ESRI ArcGIS Geographical Information System

There was a general requirement to visualize the spatial disposition of the graben relative to each other and their azimuth with the topographic features on the Martian surface; and to take measurements of the channel dimensions to determine the azimuthal changes in the channel centerlines. We needed to superimpose this information on surface images with sufficient flexibility to effectively present the data. ArcGIS spatial analysis tools and data display functions were selected. A third party ArcGIS application package “Fluvial Corridor”, developed by the CNRS research unit Lyon, was used to measure channel direction changes, (Roux et al., 2015). Alber and Piegay (2011) defined the linear reference axis (LRA) as the centerline of a fluvial feature, e.g. a channel centerline, and provided “Centerline” software in the Fluvial Corridor ArcGIS toolbox to determine the LRA from an ARC polygon of the channel floor area. Centerline achieves this by dividing the opposing edges of the polygon, representing the channel sides, into points of equal intervals and constructing Thiessen polygons between them, the polygon centers are then used to create the channel centerline, or LRA. There are usage constraints with “Centerline” where an accurate LRA is not derived and these occur at channel confluence, channel ends and abrupt changes in channel direction; these were taken into consideration and adjustments made to the LRA during the analysis.

4.1.2 CRAN application “mclust” for Gaussian Mixture analysis

The initial analysis was based on measurements of graben location and azimuth indicating the direction of dilatational stress. This produced a multimodal PDF (Fig 2) we considered to be a mixture of probability distributions; and after increasing the number of data set samples we needed a process to extract and isolate these distributions. We expected to demonstrate any organization or preference in graben spatial distribution and azimuthal direction to prove our hypothesis. As we were interested graben location (latitude and longitude) and azimuth we extracted trivariate distributions from these data. The graben population was considered to be a Gaussian mixture, as Fraley et al. (2002) had observed non-Gaussian data would often be approximated by several Gaussian ones using the methods they proposed. The R package “mclust” (Fraley & Raftery, 2006) was

used to extract the component Gaussian distributions from the graben data set to identify graben azimuth variations with spatial alignments.

The cluster selection process is started assuming the data set is a single distribution and a normal distribution model was assigned. Expectation maximization, an iterative procedure (Do & Batzoglou. 2008), was used to determine the likelihood estimator (i.e. the values of μ (mean) and σ^2 (variance)) for the selected normal distribution model that best describes the distribution data. This is repeated for all normal distribution models, and one is selected by comparing the relative performance of each using the Bayesian Information Criterion (BIC). The BIC is an index reflecting a model fit against model complexity and the most efficient model, which has the lowest BIC value, was used. The number of distributions and number of clusters was incremented and the new cluster values were selected in accordance with distance connectivity criteria. The cluster distribution selection process was then repeated. This cluster selection process can run for a default number of times or be user selected. On completion of these selection cycles, the number of clusters and distribution model type was chosen using the BIC performance index as the selection criteria. For more technical examples of expectation maximization see Chen and Gupta (2010) and for the “mclust” package description Fraley and Raftery. (2006).

The “mclust” package, written in R, provides the mean and covariance of each identified Gaussian cluster and the optimum distribution model selected by BIC, “mclust” can support up to four Gaussian distribution variables. The graphical output functions, using R graphic primitives were used to illustrate data and the data was further processed in R before export to Excel and ArcGIS.

4.1.3 CRAN application “dtw” for channel axial profile matching

In matching channel direction changes with graben orientation it was necessary to accurately identify common sequences of the linear reference axis (LRA) azimuth changes between the channels considered. The channel LRA was subdivided into equal segments and the key data was channel measurement position and azimuth at that sample point. The segmented LRA for each channel was used for the comparison. To demonstrate a match or degree of match between channel profiles is relatively straight forward using channel direction changes (azimuth) and regression techniques if they are of the same length, and equivalent points occur on the same position along the interpolant. We wished to prove the shape of the channel direction profiles matched between channels of different lengths, with different feature interspacing, similar shaped features, whose data (azimuth) varied over near identical range of values. We needed a method of channel comparison that would compare the overall shape and not provide an equivalent point-by-point comparison. “dtw”, a CRAN application (Giorgino, 2009) is able to compare two time or spatial ordered series of different lengths and determine the degree of match between them using the dynamic time warping DTW method. The software package “dtw” was used to identify channel sections of similar shape and orientation. DTW is a mature analytic technique used extensively in analyzing time and spatially ordered series across a variety of applications including, for example, speech recognition (Rabiner & Juang, 2008), gene time series analysis (Criel & Tsiporkova, 2005), handwriting recognition (Rath & ManMatha, 2003) and chromatography (Wang & Isenhour, 1987).

DTW projects one of the channel profiles as ordinate (y) the other as abscissa (x) onto an interpolant angled at 45 deg to the origin. The interpolant is called the warping axis. DTW moves a projected x or y value along the warping axis to co-align equivalent points, extending the axis when required

This movement is achieved by inserting a data point value before the point of interest, by shifting the point of data and all subsequent data along the axis away from the origin to make a space. Equivalent points are a point pairs of x and y values where the Euclidean distance between, the residual error, is very small ideally zero. The data inserted into the space is the value of the last xy pair, which achieved a match, and this value persists until another xy match is achieved. By repeating this process, and applying sets of rules, the variations in channel feature displacements and differences in profile lengths are accommodated and result in the alignment of equivalent points along the common warping axis; this result is called the warping function. The warping function provides a mapping between equivalent points on the x and y axes,

The DTW performance metric, Normalized Distance (ND), is an indicator of match; this is a normalized aggregation of the sum of the residual errors. Because of the small number of channels we have available the relative meaning ND between channels is not readily demonstrable. Instead, we use linear regression techniques and performance indices on the warping function as the equivalent points are now aligned. The degree fit is measured using r^2 and Pearson's R as these are understood and proven.

The effect on the regression of inserted data into the channel profiles by "dtw" has been evaluated using standard regression diagnostics including, residuals vs. fitted tests for residuals non linearity and outlier identification; normal Q-Q to test residual normality; scale vs. location to test evenness of spread between residuals and predictors; residuals vs leverage (Cook's test) to check for influence of outliers on the results; and heteroskedasticity, the systematic variation in the size of the residuals. Our results passed these tests and the values of r^2 and Pearson's R are considered valid and they indicated a satisfactory match so we consider the outcomes of sufficient accuracy for the purpose of the study. The influence of the extra data on the final results has been shown to be insignificant within the context of our requirements. DTW does not have an equivalent set of data diagnostics.

The DTW convention is to compare unknowns, or "queries" against a standard or "reference". Channel 1 was assigned as the reference and all other channels assigned as the query, and in our case we selected the option to move both reference and query points on the warping axis to achieve a match (Tormene et al., 2009). As the channel samples were limited we simulated test data sets to determine the most appropriate warping settings (Keog & Pazzani, 2001).

The "dtw" application provides graphical outputs of the results, with full access to the warping outcome data and the internal data sets supporting the warping process. Data was exported using R code for input to Excel and ArcGIS.

4.2 Graben Analysis workflow

This section outlines the workflow and packages used to produce the graben azimuth data for analysis. At study initiation an initial data set containing the location and orientation of a sample of graben was measured and a preliminary analysis performed as a test of the hypothesis that graben were arranged in groups and their directions orientated to surface features or another direction in an organized manner. Given the successful test outcome the data set was then expanded to include the remaining graben in the study area

The graben data set was generated in an ArcGIS table using ARC tools. First a straight line from graben tip to tip was drawn and a perpendicular at the line midpoint created, and from this the azimuth of the line determined. This azimuth, i.e. the graben azimuth, location and other table attributes were added to assist analysis and display.

The initial dataset of 342 samples (Fig 2(a)) was exported to an R application to create the graben azimuth Probability Density Function (PDF) as in Fig 2(b); which has three distinct maxima comprising 5 modes and the graben from each mode are shown in the locations in Fig 2(c). Using ArcGIS, the graben for each mode, and a symmetrical range about their mean, were manually selected to visualize the surface location of every graben within that mode. With the exclusion of some outliers, it was found that each mode contained clusters of points which were either spatially associated with large surface features, assuming a dilatational environment; or had common spatial alignments with a similar azimuth. The outliers were attributed to the coarse method of graben selection. Fig 2(c) visualizes the PDF segmented according to the selected mode. As a result of this manual test we increased the graben sample size to 845 by extending the mapping range and subdividing some previously mapped graben. This became the baseline data set and the PDF for this is given in Fig 3(a). Fig 3(a) shows the relationship between the graben azimuth and the PDF; and to illustrate how the graben spatial aggregations contribute we show the graben spatial distributions in Fig 3(b), and how they summate into the PDF

The CRAN package “mclust” minimized bias and increased accuracy during the cluster extraction. The Gaussian distribution was chosen for reasons already given and “mclust” resolved 24 clusters. Using ArcGIS many of these were spatially aligned with surface features. Some clusters were multimodal, and where possible, these were subdivided into subclusters. The clusters and subclusters, were imported into ArcGIS and the spatial center, and mean azimuth of each cluster was calculated and visualized, Fig 4 (a), and the stress tensor map derived by Hall et al. (1986), Fig 4(b) is provided for comparison,

The values of the cluster means were projected in ArcGIS to determine if it targeted volcanic structures or other tectonic feature. For effective visualization the boundaries of the volcanic structures were defined as the break in slope of the edifice onto their supporting surface and these are shown as different colored boundaries (Fig 4 (a)). The color-coding aided recognition and each graben cluster member was visualized in ArcGIS as a

rhombic shape and color matched to the identified target. (Fig 4(a)). The arrows representing each cluster mean were also matched to the target color.

To provide clarity and assist the reader, these data were temporarily labeled in the paper according to their apparent target: NWSE = linear array of graben pointing either NE or SW (brown); HTnorth graben cluster members focused on the north side of Hecates Tholus (HT) (green) or proximal to it; HTsouth graben cluster members focused on the south side of HT or proximal to it; AT graben cluster members focused on Albor Tholus (red), EM graben cluster members focused on Elysium Mons (blue) ; and SER graben cluster members focused in directions to the south east region (yellow) and not directly at EM.

Crosscutting graben were identified by visual inspection, and their locations mapped and marked in ArcGIS with an identifier (Fig 5(a)). Each cross cutting pair was examined and their association with a particular source of stress verified by graben azimuth projection (refer to S1). These relationships were tabulated (Fig 5(b)) and summarized (Fig 5(c) and Fig 5(d)).

This workflow produced an ArcGIS image with each graben location color-coded to a target area; with the cluster mean azimuth arrows indicating direction. The cross cutting locations and their crosscutting order was evaluated and recorded (Fig. 5). Also produced were maps showing the location length and orientation of each graben and some intermediate analysis data plotted spatially for reference.

4.3 Channel Analysis workflow

This section provides a description of channel data workflow, which is followed by a description of the channel spatial analysis. Initially the channel profiles were compared using manually generated ArcGIS profiles and these data transferred to Excel for analysis. From these results, similarities in channel centerline azimuth were identified, in particular between Channels 1, 2, 6, 7 and Channel 8. Channel 1 was chosen as the reference for comparison as this was considered the best representation of channel morphology, and was judged to be the most clearly defined. Further analysis was then undertaken on all channels using DTW with LRA data generated using ArcTools..

Derivation of the channel Linear Reference Axis (LRA) with the Fluvial Corridor centerline utility requires a definition of the channel floor expressed as an ARC polygon, shown as a colored area on the channel floors (Fig 6 and Fig 7). There are morphological and channel floor deposit differences between the channels, so an unambiguous definition of the channel floor boundary was required, although this was not straightforward; the following thought-process led to the chosen scenario. Estimation of the channel wall base contact through the colluvial deposits was discounted on the grounds of accuracy, repeatability and the variability of depositional conditions between channels. Similarly, the upper colluvium contact was considered but discounted due to its obscurity in many channel sections. The channel boundary contact was defined as the channel floor contact with the base of the colluvial deposits, which is generally visible and so repeatable and objective. This excludes other

channel floor deposits and debris. It is accepted that this contact has been subject to aeolian and possibly fluvial erosion, but in the majority of cases the channel lengths have opposing colluvial deposits of similar widths, which are small compared to channel width, thus minimizing the centerline error.

The activity sequence to produce a channel LRA data set was started by creating an ArcGIS channel floor polygon, which was then processed by Fluvial Corridor Centerline creating an ArcGIS polyline of the channel centerline. Using ARC tools this polyline (LRA) was divided into 100 m long sections, and the azimuth of each 100 m section determined for the complete channel length. A series of marker points spaced 0.5 km apart were created along the LRA from channel mouth to head. A moving average about each marker point was calculated using the 100 m linear data segments in a range ± 0.25 km about each, so providing data smoothing. Channel LRA azimuths vs. distance datasets were created for each channel using this method. Adjustments were made to the LRA to compensate for algorithmic distortion at the LRA terminal points, instances of rapid directional change and at channel confluences by eliminating selected outliers (Roux et al., 2013)

The DTW convention is to compare unknown profiles, or queries, against a standard profile, or reference. DTW rules require optimization to assure “DTW” discrimination sensitivity for the shape of the profiles being compared. As the study samples were limited in number, test profiles were generated by simulating randomly placed Gaussian distributions of changes within a copy of the reference profile, Channel 1, which was used as the query and compared with the unchanged Channel 1 data. For each set of “DTW” rules 1000 randomized test profiles were generated automatically and each of these query variants were matched with the reference and the results recorded. From each set of results the mean value of ND, r^2 and Pearson’s R values were calculated and the rule set with the lowest of these metrics was selected. During this process the LRA data binning was adjusted to 200 bins minimizing the effects of data noise, and a degradation of feature discrimination noted between channels of significantly different lengths.

Though “dtw” provides Normalized Distance (ND) as a measure of success we used linear regression using warped data to measure the degree of match for the reasons given above. The outcomes of DTW and the linear regression are shown in Figs 8 and Fig 9.

Each channel was compared with the reference, but Channels 3, 4 and 5 did not match even though they share the same morphology as Channel 1 as they lack any of the major azimuth deviation features.

After channel matching equivalent sections of azimuthal profile or “stages” were identified between them. The azimuth mean value of each stage, for Channels 1, 2, 6 and 8 were calculated and the perpendicular to each of these directions was constructed at the stage midpoint on the LRA (Fig 10). For all channels in Fig 10 the perpendicular at the center of each stage azimuth mean line is indicated with yellow filled arrow to indicate the direction of dilatational stress and a line arrowhead was used to indicate the direction of average stage azimuth

5 Data

This section identifies the source of Mars surface images and DEMs and provides technical references of the instruments used.

The images used in the analysis have primarily been obtained from the Context Camera (CTX), resolution ~6 m/pixel, Malin et al., (2007), because High Resolution Imaging Science Experiment (HiRISE), resolution up to 0.25 m/pixel, camera images (Delamere, 2010) are not available for most of the region studied. HiRISE and CTX are on the Mars Reconnaissance Orbiter (MRO) satellite. Where there are gaps in the CTX image coverage, images from the Mars Express (MEX), High Resolution Stereo Camera (HRSC), up to 12.5 m/pixel, were employed, (Neukum, 2004). Larger scale areal views were obtained from the Mars Odyssey satellite (MO) Thermal Emission Imaging System (THEMIS), 1km/pixel, daytime images as they provide a consistent presentation of sufficient detail across large areas (Christensen et al., 2004). With the exception of HRSC images all other images were obtained from the NASA Planetary Data System (PDS) Node; HRSC images were obtained from the ESA Planetary Science Archive (PSA). Surface elevation data can be obtained from several sources, however Mars Orbiter Laser Altimeter (MOLA) data were used throughout. Accurate measurements were obtained on a per point basis using individual shot data from MOLA PEDR files.

6 Results

This section first describes results from the graben analysis followed by the outcomes from the channel investigations. These results are then reviewed together to determine if there is a match.

6.1 Graben

6.1.1 Results Review

The results of the graben analysis for the NW quadrant are summarized in (Fig 4a) and the following observations can be made.

The graben categorized as NWSE (brown) are arranged in bands orientated in a NW to SE zone in the north of the study area; these are members of PDF mode 1 (Fig 3(b)). A comparison with a clusters of other regional graben to the SE of EM, includes the most western sections of Cerberus Fossae, show an equivalence in their azimuthal distributions (Fig 3(c) and Fig 3(d)) showing binned (2.5 deg) frequency distributions, matching in shape, with maximum for the SE in the 27.5 -30 range (Fig 3c) and the maximum in NW in the 30-32.5 range (Fig 3d). From these data we concluded the frequency distributions matched and the graben were generated by the same influence even though there was a slight change in maximum value.

The azimuth pointers for HT graben (green) vary in their orientation from west to east maintaining a focus on the center of HT. Within the HT population are two distinct, sub-clusters, which are grouped by area and linearly aligned. One cluster points to the south of HT (HTs) and the area beyond and the other set directly towards HT and north of HT (HTn). These graben lie in bands from 345 to 410 km from the edifice center and interleave with NWSE clusters in the NW quadrant.

The graben azimuth directed towards Elysium Mons EM (blue) define arcs of concentric rings whose radii converge in the direction of EM, these are in PDF mode 2 and 3 (Fig 3b). There is a higher density of arcs and graben between 196 km to 225 km in radius. Traversing each graben arc, the individual azimuth adjusts to maintain convergence on a common focal point. However, the location of the common focal point is different for each arc and moves in a direction NW as the arc radius increases. These arc segments are components of series concentric rings which lie within a band 150km \pm 20km to 350km \pm 20km as observed by Comer (1985), and Hall et al. (1986).

A few graben azimuth (Fig 4(a)) are directed towards Albor Tholus AT (red) rather than the EM edifice axis. These clusters are members of PDF mode 2, Fig 3(b). However the mass of AT is considered insignificant to that of EM, HT and the Elysium Rise (Hall et al., 1987), and it is implausible any radial magma flows or stress from the AT edifice area would have passed by the NW flanks of EM to those graben locations, consequently we suggest these graben are subsumed into SER in the following analyses.

The majority of graben interpreted to point towards the Southern Elysium Region (SER) (yellow) are in PDF mode 3 (Fig 3(b)) with an outlier in mode 2. Within SER are grouped and arcuate bands of graben that do not conform to the preceding classifications. The end on end alignment of graben form segments of arcs which are not concentric around EM, and the azimuth of clustered graben deviate substantially from focusing on the EM axis. These azimuths do not point to obvious features or regions of stress.

In summary, and with the exception of SER, graben clusters associated with HT and EM adjust their mean azimuth to create a focal point around or near to a volcano central axis, however the HT graben are linearly aligned and in contrast the EM graben are concentric about the edifice axis. The HT and EM graben clusters are proximal to their respective load centers and crosscut each other in the NE of the region. EM has a variation in concentric graben density, the most closely packed graben are the more distal from the edifice axis. NWSE clusters are quasi – linearly aligned and this alignment extends to other, larger clusters in the SE of the region. SER graben cluster azimuth point away from the EM axis and the linearly aligned graben loci appear to be more ellipsoidal than their concentric circular EM counterparts.

6.1.2 Inferred stress field variation through time

This section describes the crosscutting relationships between graben within the study area and the methods used to determine the existence of a sequence of stress related events. From the cross-cutting observations and measurements (Fig. 5(a)) a time ordered progression of cross cutting events is derived as follows:

The NWSE graben are the start of the crosscutting sequence;

NWSE graben are crosscut by HTs graben;

HTs are crosscut by HTn graben (see note);

HTs are crosscut by SER graben; and

SER are crosscut by EM graben.

Note:

The HTs crosscut by HTn is only seen clearly at location 2 and it has not been possible to discriminate between HTs graben before or after this event. (Fig 5a).

The crosscutting sequence is from oldest to youngest.

This sequence (Fig 5(b)) shows a detailed crosscutting progression from the oldest, NWSE through to the youngest, EM, and the transitions associated with AT are subsumed into SER for the reasons given. A summary of this sequence is provided in Fig 5 (c) and (d).

These cross cutting relationships can be re-expressed in terms of direction change starting from NWSE. The sequence is: turn clockwise southwards, turn anticlockwise northwards, turn clockwise southwards then turn anticlockwise. This sequence reflects the major changes in stress field direction through time from different sources. The graben cluster azimuth of HT and EM so aligned they converge on or near the center of these edifices inferring a possible dilatational, σ_3 environment. In contrast NWSE graben are linearly aligned NW-SE, an alignment that also occurs in the SE of the region (Fig 1(b)) and could have been created by either σ_3 or σ_1 as previously discussed (Section 3.3)

6.2 Channel analysis

The results from the channel analyses are discussed below and these are generalized into a form for comparison with the regional stress variations implied by the graben orientations. The comparisons are between Channel 1 (Fig 6(a) and (b)) and Channel 2 (Fig 6(c) and (d)), Channel 1 and Channel 6 (Fig 7(i) and (j)), and Channel 1 and Channel 7 (Fig 7(g) and (h)), and finally Channel 1 and Channel 8 (Fig 7(g) and (h)).

6.2.1 Channel 1 and 2 comparison

The comparisons between Channel 1 and Channel 2 are described in greater detail below, with the remaining results provided in a more summarized form.

Visually comparing Channels 1 and 2 (refer Fig 6 (b) and (d) and Fig 8 (a) and (b)) and referring to the bin numbers: from bin 0 the azimuth profile decreases to an inflexion, next rising and then decreasing further to a minimum near bin 60. From bin 60, which is larger for channel 2, the profile increases to a maximum near bin 80. From bin 80 to 120 Channel 1 has a well developed maximum region whereas Channel 2 it is less so; from bin 120 both profiles then decline toward bin 140 rising again to bin 150; and from there both profiles remain relatively constant, except for small perturbations until bin 180 where there is a minimum.

The post warping graphs show values interposed between measurements to spatially align equivalent profile segments on the warping axis Fig 8(c) and Fig 8(d). The three-way plot (Fig 8(f)) summarizes the matching process, where the vertical and horizontal steps in the diagonal profile, the warping plot, show the shifting of the query values (Channel 2) or reference (Channel 1) values by inserting the last value measured prior to mismatch to align equivalent points between channels along the shared axis. The distance between the equivalent points is summated and normalized to produce the Normalized Distance (ND), where the magnitude of ND indicates the degree of mismatch, for an ideal match $ND = 0$. The fine dotted lines (Fig 8(f)) identify some equivalent points of the reference and query and their spacing indicates the relative movement between profiles.

Post-warping Channel 1 and 2 match well with a low $ND = 4.42$. The linear regression scatterplot shows a close distribution of points and the injected points can be seen as either linear vertical or horizontal arrays of data points (Fig 8(e)). Channel 1 and 2 show good correlation ($r^2 = 0.873$), and they are normally distributed with no obvious outliers influencing the regression; Pearson's $R = 0.919$ to 0.946 (95% confidence). The LRA azimuthal variations show a long period variation with superimposed shorter period deviations (Fig 8(c) and 8(d)).

In many cases the shorter period variations also match between channels providing a good channel match. Note a match has not been fully achieved where a section of (injected) data on the warping axis in one channel profile opposes an unaltered section of profile in the other. The injection of the last matched point value when warping for alignment has the effect of creating a slowly changing profile when there is a series of very short inter-dispersed matching sections with no match between them. Consequently a detailed match of a channel profile section may not be achieved however the linear regression residuals for that section will be minimized. The value of ND reflects the degree of match and a value less than 10 is considered to be good. ND like r^2 should be treated as an indicator of fit since the range that the value is in is of importance not necessarily the value itself.

The detailed matches between Channel 1 and Channel 2 identified seven channel sub-divisions referred to as stages (Fig 6 (a) and (c)). Each stage was defined by the point of a major directional change of channel azimuth Fig 6 ((b) and (d))

6.2.2 Channel 1 and 6 comparison

Channels 1 and 6, Fig 6 (a) and (b) and (Fig 7(i) and (j)) showed similarities pre-warping (Fig 8(g) and (h)), and the post-warping profiles (Fig 8(i) and (j)) show no matches up to bin 90 of Channel 6, this feature is also shown in the three-way plot (Fig 8(l)). Channel 1 and 6, match with $r^2 = 0.692$, Pearson's $R = 0.786$ to 0.831 (95% Confidence) and $ND = 5.46$. The Channel 1 and 6 regression is linear, normally distributed with no influence from outliers (Fig 8(k)). The comparison shows matching with stages S2, S3, S4 and S6 of Channel 1. Matching features in Stages 1 and 5 were not detected and this factor and the large non-matching channel section up to bin 90 will have suppressed the values of r^2 and Pearson's R . As DTW had eliminated the effects of channel propagation rates it was considered reasonable to include Channel 6 even though it is much shorter than the others.

6.2.3 Channel 1 and 7 comparison

Comparing Channel 1 Fig 6 (a) and (b) and the shorter Channel 7 (Fig 7(g) and (h), Fig 9(a), Fig 9(b)) pre-warping show no obvious matches. Post-warping Channel 1 profile has been shifted significantly to align only stage 1 and stage 2 with the complete section of Channel 7 profile (Fig 9(c) and (d)). The three way plot (Fig 9(f)) shows some matching in the first third of the reference; $r^2 = 0.7373$, $ND = 3.64$, and Pearson's $R = 0.825$ to 1.00 (95% confidence) Channel 1 and 7 regression is linear, with no obvious outliers, Fig 9(e). We observed that only part of stage 1 and some of stage 2 achieved a match using a small number of equivalent points within large regions of unmatched flat channel sections, which slowly track the variations tending to minimize the residuals. The paucity of detailed matching features makes a conclusive match less certain, so Channel 7 was not considered further even though the matching indices are acceptable.

6.2.4 Channel 1 and 8 comparison

There are significant morphological differences between Channel 1 and 8 and initially "DTW" did not give a match. Referring to Fig 6(f), two sections were excluded, first from 0 – 10km, was excluded as a local topographic anomaly not seen in the other channels. Secondly, the section from 115km – 145km was considered as a separate channel as shown in Fig 4(f). This section is bifurcated, therefore unique, and the upper channel has separate surface flow channels to the south. We concluded the channel midsection had migrated up stream breaking into the upper section during its development.

Channel 1 and 8 showed some equivalent features Fig 9(g) and (h), even though the degree and rate of azimuthal change in Channel 8 is much greater than Channel 1. The post warping profiles Fig 9(i) and 9(j) showed matching between the main features in Stages S1, S3, S4, and S5 (Fig 9 (l)) however there are fewer equivalent points in the stages 2 and 6. Regression of Channel 1 and 8 Fig 9(k) showed deviation from normality in the upper and lower variable range in particular above 120 deg. azimuth, however these are not seen to influence results; $r^2 = 0.78$, and Pearson's $R = 0.86$ to 0.9 – 95% confidence

6.2.5 Channel Data Summary

The channel results are summarized below showing the normalized distance (ND) metric calculated by “dtw”; the value of Pearson’s R quoted at 95% confidence levels; the linear regression metric r^2 and the number of stages matching the reference (Channel 1).

Channel 1 and 2: ND= 4.40, PR = 0.919 to 0.946, r^2 = 0.87, stages S1, S2, S3, S4, S5, S6, S7;

Channel 1 and 6: ND= 5.45, PR = 0.786 to 0.831, r^2 = 0.69, stages S2, S3, S4, S6;

Channel 1 and 7: ND= 3.64, PR = 0.825 to 1.00, r^2 = 0.74, stages S1, S2, and

Channel 1 and 8: ND= 6.61, PR = 0.860 to 0.90, r^2 = 0.78, stages S1, S2, S4, S5.

Channels 1,2 and 6 have the same morphology and the matches occur between the majorities of equivalent points. Channel 1 and 7 correlate well but comparing Stage 1 and Stage 2 only, and matching is only between a few equivalent points interspersed by large gaps of inserted data making the match less conclusive and therefore excluded from further consideration. Channel 8 morphology is rille -like and Channel 1 is theatre headed -like, however Channel 8 LRA correlates well with the LRA of Channel 1 over several channel stages.

In the analysis of channels 3, 4 and 5 (Fig 7 (a), (b), (c), (d), (e), (f) respectively) “dtw” failed to find a match so these channels are not included in any further analysis.

From the above we concluded all matched channels have the same LRA including the rille-like Channel 8.

6.2.6 Channel Axial Variations

The detailed matching between channel stages has been shown; however the average stage azimuth was used to demonstrate coherence between channel direction changes and changes in the regional stress distributions since the regional stress change sequence is less refined. The stage average azimuth was calculated from channel azimuth data, for Channels 1, 2, 6, & 8, excluding channels 3, 4, 5 and 7 for the reasons given. We then considered the average azimuth changes between the stages for each channel, and generalized the changes as clockwise for an increase in azimuth, southwards, from one stage to the next, referenced to north, and anticlockwise as a reduction in azimuth from one stage to the next, northwards. This approach allowed us to express changes in slope direction rather than comparing absolute values making comparison easier. Consider the transitions in Channel 1 (Table 2), starting from Stage 1 and moving up-dip from channel mouth to channel head (Fig 10(a) and 10(b)).

The progression in channel changes include:

Stage 1 azimuth changes clockwise to Stage 2 azimuth;
Stage 2 azimuth changes further clockwise to the Stage 3 azimuth;
Stage 3 azimuth changes anticlockwise to the Stage 4 azimuth;
Stage 4 azimuth changes anticlockwise to the Stage 5 azimuth;
Stage 5 azimuth changes clockwise to the Stage 6 azimuth, and
Stage 6 azimuth changes anticlockwise to the Stage 7 azimuth.

This sequence was derived for other channels and then compared. Similarly, we then derived the sequence for channel growth down dip from head to mouth (Fig 10(c)).

With the exception of channel 8, all channel direction changes matched for each direction of channel growth (Fig 10(b) and Fig 10(c)), the Channel 8 differences are shown in red. In some channels the general direction is maintained between successive stages, for example stages 2 and 3 in Fig 10(b). We suggest these small changes in azimuth infer flow events occurring under similar erosional conditions and controls including little change in regional stress fields. These successive changes were combined resulting in a sequence head to mouth as clockwise, anticlockwise, clockwise and anticlockwise for both directions of channel growth. Channel 8 has an additional change in azimuth at the mouth, Fig 10(d) and Fig 10(e) due to the magnitude of the stage 2 transitions.

6.2.7 Channel direction and graben cross cutting sequence matching.

To demonstrate the similarity between stress field direction changes, inferred from the graben cross cutting sequence and channel direction changes we consider the possible development controls over the channel area and these, included slope gradient and dilatational stress.

An erosional environment is required for channel creation and requires flow with either lava, water or water mediated material flow as the likely agents, and these are considered to have existed from the Late Noachian to the late Amazonian Periods (Howard et al., 2005, & Carr and Clow (1981), & Christiansen, 1989 & Tanaka et al., 1992 & Russell and Head, 2003, & Madeleine et al., 2009). The Elysium Rise gradient is less than 1°, and at these gradients other factors, for example lava, debris flow or aeolian deposits, and surface features including channels, fissures or graben will have increased influence on flow direction. To achieve the channel direction matches demonstrated between the channels relying only on the direction of maximum slope would require a region wide influence on slope gradient, locally adjusted to accommodate dissimilarities in pre-flow gradient profiles, overcome surface deposits and features and yet produced matching profiles in this low energy flow environment. We consider this possibility unlikely considering the factors above and propose the presence of tectonically created features to achieve channel matching.

Fault control is associated theatre-headed morphologies (Laity and Malin, 1985 & Lamb et al., 2006 & Lamb et al., 2014, & Schultz et al., 2007). For maximum effect in influencing channel direction change the stress has to

act either perpendicular to or parallel with the graben axis, which in-turn controls the channel direction. These effects constrain the stress source relative position to the channel; for example, assuming the channel develops up-dip from mouth to head, the Channel 1 channel azimuth perpendiculars in the order below (Fig 10).

Initially Stage 1 points to the NWSE graben in the study area;
Stage 1 changes clockwise to Stage 2, S to NWSE region;
Stage 2 changes clockwise to Stage 3, further S to HT (HTs);
Stage 3 changes anticlockwise to Stage 4, N to HT (HTn);
Stage 4 changes anticlockwise to Stage 5, further N to HTn;
Stage 5 changes clockwise to Stage 6, southwards to HTn; and finally
Stage 6 azimuth changes anticlockwise to Stage 7 and this azimuth perpendicular moves to the north of HTn.

In summary, the azimuth perpendicular axes in steps 1 to 5 vary in the directions towards the NWSE graben strings and HT and this sequence of direction changes compares favorably with the first three changes in the regional stress field changes inferred from the graben cross cutting in Fig 5(c). In this case the channel wall direction, parallel with the graben direction, is fault controlled and step 6 and step 7 could reflect further changes in the stress fields generated by NWSE or HT. However, stress directions related to SER and EM are more likely to act on the channel heads (Lamb, 2014) and in this case step 6 azimuth would point in the same direction as SER and step 7 channel azimuth point in the direction of EM. In these cases faulting is perpendicular to the channel axis at the channel head and controls the direction of channel development. So step 6 and step 7 then match the changes in the later stress field variations observed in graben cross cutting sequence i.e. from HTs to SER returning to EM, Fig 5(d).

This analysis shows a match can be achieved between the channel direction change sequence and the variations in the graben cross cutting sequence, thus inferring stress change over time controlling the channel direction. However this is provided two constraints are met, first, this match is conditional on the channel developing from mouth to head. Second, fault control on the channel walls influences the early development of channels (step 1 to step 5) but the control changes to faulting and jointing controlling the direction from the channel head (step 6 and step 7). A match cannot be achieved if the channel is considered to develop from head to mouth.

Similarities in the slope gradient during the initial stages of channel erosion cannot be assumed so initial channel directions may differ, however, as the channel deepens fault control would become more dominant as the floor gradient reduces and mass wasting proceeds.

Matching channels include both theater headed and rille-like morphologies, however we identified earlier (Section 3.4) that arcuate and linear rille development direction cannot be generally predicted but these developments occur within the orientation of the stress field prevailing at the time. Therefore the order of development of the fissures, graben, or dike emplacements can occur in any order within a straight section of rille. However when the next stage of the rille is formed with a different stress orientation the growth needs to be from the head of the previous section. This migration upslope could be achieved either by an eccentric dike,

as defined by Acocella (2001) migrating upslope if that was the general behavior or by a radial dike migrating upslope. The FEM models of Hurwitz et al., (2008) and Galgana et al. (2013) both showed the radial dike flow is vertically constrained at the contact between the edifice and the upper crust. So as the province inflated and flank deposition continued it is possible that the radial dike conduits increased in elevation.

From above (Section 3.4), the theatre headed channels require an aqueous source for development within a stress regime similar to that influencing Channel 8, whose development is dependent on volcanic processes for its creation. This implies coeval activity of these two erosional processes producing matching channels under similar tectonic conditions, an occurrence considered unlikely. Considering the channel morphologies (Supplement S1); Channel 1 is theatre headed like; Channel 2 has a theatre headed like lower section with narrower sinuous upper section; Channel 6 is a much narrower and theater head like and similar in width to Channel 8; and Channel 8 is thin and arcuate rille-like; which suggests a mix of morphologies amongst them. It is proposed that all matching channels were initially rille-like and some transformed to theatre headed morphology later by mass wasting. This is based on the assumptions the occurrence of coeval erosional events is unlikely and the mix in channel morphologies observed. This would require the presence of water after final stage volcanism, which is possible from synvolcanic melting of sub surface ice or snow (Madeine, 2009 & Christiansen, 1989 & Tanaka et al, 1992, & Russell and Head, 2003). This reuse of existing channels by other erosional events on Mars has already proposed by Gulick (2001).

7 Discussion

In this study we have shown that there is a spatial and directional relationship between graben, the volcanic edifices and other tectonic features in the study area. We have also shown that there is a correlation between changes in channel direction and regional stress variations over time; and demonstrated that there is commonality in channel axial direction change between rille-like and theatre-headed like channel morphologies. In this section we will investigate the implications of these observations.

We now consider the stress distributions derived by Hall et al. (1986). Our models differ in their base data and processing however there is commonality in some of the analysis outcomes. Hall used gravity, topography and a thin elastic shell flexure model to determine a regional stress distribution, which they then reconciled with the regional tectonic features. Our model was based on tectonic feature mapping and analysis of their attributes. Hall (1986, their Fig 12) included the superposition of EM and HT loading, regional uplift and Tharsis Montes isostatic and flexural stress on the lithosphere in the synthesis of their results. Our mapped model made no assumptions on stress sources and their location, and we analyzed these data and based our observations and conclusions on these results.

There is coincidence between the results of Hall et al., (1986) and our observations of the concentric rings around EM, and the graben clusters pointing in the direction of HT. Hall et al. (1986) showed an offset in the

EM center of mass from the caldera towards the NW, an observation shared by Janle and Ropers (1983). We observed the concentric graben rings focal points moving away from the center of EM as the concentric graben arc diameters increased. This shift in graben focus away from the EM axis could be interpreted as a shift in the center of mass (principles established by Comer et al. (1985). We note this observation as a possible indication of increasing center of mass offset from EM developing during volcanic activity, however further analysis is required to substantiate this proposition. Hall et al. (1986) does not account for the NWSE graben but suggests they are formed either by un-modeled asymmetries in the uplift model or local lithospheric heterogeneities, creating fractures by thinning. Hall et al. (1986) and Banerdt et al. (1982) considered their isostatic model of Tharsis generated stress in our study area, and this is used to account for the formation of Cerberus Fossae (Fig 1b), which have the same NW to SE orientation as the NWSE graben. Our results suggest the Cerberus Fossae graben are similar to those elsewhere in the SE Quadrant and those seen in the NW Quadrant, Fig 1(b). If this is the case these observations contradict Hall et al. (1986) and Bandert et al (1982) as it is thought the main Tharsis activity occurred after the growth of EM (Werner, 2009) and the NWSE graben precede the EM graben in the graben crosscutting sequence. We suggest that the NWSE graben are more likely to be the consequence of regional uplift, and are formed by plume related extensional uplift with σ_3 acting horizontally in the NE or SW direction; alternatively a large σ_1 stress could have acted vertically within an horizontally constrained crust and produce similar features. The absence of the southerly band of NWSE graben, and other graben, in the western regions of the NW quadrant is distinctive, however the explanation for this absence is beyond the scope of this paper. Hall et al., (1986) does not identify stress sources associated with the SER graben set.

We now compare our results with the conclusions drawn from FEM modeling, however an FEM model for the Elysium Province has not been available for comparison and our comments are based on generalized models. We consider some of the outcomes of previous work and others in the following paragraphs, and from these observations we suggest a possible development sequence for the Elysium Province.

From our observations we note that EM and AT are confined between the northerly and southerly NWSE graben bands whereas HT lies outside and to the north of this fracture zone. The preferential development of EM over HT could be due to magma rising between the N and S, NWSE graben bands boundaries or the HT magma feeder dikes could have been diverted by EM lithospheric loading (Muller et al., 2001). AT appears as a flank cone on the SE flank of EM.

The conditions for the creation of the linear clusters HTn and HTs are now considered. The absence of concentric graben around HT could be due to several factors including; insufficient loading to create lithospheric flexure capable of creating graben; their burial as the EM edifice developed; or the distance of HT graben from the HT vertical axis of symmetry. The EM concentric graben occur within a zone equivalent to the radius of the edifice outwards from the stratocone periphery Fig 3(e); whereas the HT, graben begin to occur beyond three HT radii and they are not concentrically aligned. It is considered unlikely that flexure would occur at this distance about HT for this relatively small edifice basal diameter and mass. This assumption is supported by comparing Fig 3(d) and Fig 3(e), which show two different volcanic scenarios each providing the same distance relationship. One scenario is EM (Comer, 1985), and the other, a volcano on Venus (Galgana et al.,

2013) and in each case the region of maximum dilatational stress on the forebulge peak occurs at a distance, approximately equal to an edifice radius, from the edifice periphery as shown. It is suggested as unlikely that HT loading would be the primary cause for the creation of HTs and HTn graben.

We consider two scenarios for the development of HT graben; a radial dike swarm or the influence of HT related stress during NWSE graben development. Radial dike swarms have been shown to occur when the main volcano conduit is blocked (Hurwitz et al., 2009 & Galgana et al., 2013) promoting radial lava flow. HT graben crosscut each other implying multiple events, which is consistent with the observations of Galgana (2013) whose time stepped analysis identified cyclical successions of central conduit blockages generating episodes of radial lava discharge. The HT graben strings can be seen to tend towards parallelism with the NWSE graben bands distally from the EM edifice in the upper western area of the NW quadrant (Fig 4a). This radial graben configuration is consistent with the observations of others, for example Ernst et al., 2001, where graben emanate radially from the edifice center aligning distally with regional stress influences. An alternative hypothesis is that while the NWSE graben are created by the regional stress fields; they are also influenced by the stresses related to HT development. We consider this unlikely, first HT is N of the northern NWSE band of regional fractures and as such any HT generated σ_3 stress would be likely to be accommodated within northern fracture zone. Second, it is unlikely HT could directly influence regional vertical σ_1 stress due to the fracture zone. These factors, and the distance of HT from the HTn and HTs graben which we have previously discussed, plus the relative timing of HT graben creation indicated by the cross cutting sequence, make it unlikely HT was an influence in the creation of the NWSE graben. In conclusion we consider graben we assigned to HT are likely to be dike swarms acting radially from the EM edifice and tending to the regional stress tensor distally. The diversion of conduit flow to radial flow requires the edifice to have accreted sufficient mass for that to occur implying their formation possibly mid to late stage EM stratocone development.

The concentric graben about EM are consistent with the lithospheric flexure models of Hall et al, (1986), Comer et al. (1985), and Galagana (2013). These graben are not radially distributed in a uniform manner but are arranged as concentric clusters of graben with varying interspaces and graben density; the possible cause of these features will now be discussed. The shallow magma chamber Fig 3(f) shows a forebulge maximum at twice the edifice radius from the edifice axis with a distinguishable maximum, similar to Comer, 1985, and the forebulge predicted for the deeper magma chamber is beyond the two-radius limit with little bulge visible. We propose that a shallower magma chamber and/or a smaller T_e produce a more pronounced forebulge since they have greater influence on the lithosphere upper boundary, which is consistent with the models of Grosfils, (2007), Hurwitz et al., (2009), Galgana et al., (2011), and Galgana et al., (2013).

The bands of concentric graben about EM (Fig. 4) could represent episodes of growth if the preference for graben development occurred primarily in the region of maximum dilatational stress, the forebulge. This argument is consistent with the multiple events of radial dike swarms discussed above; provided there is sufficient dwell time between these radial flow events to allow edifice accretion and renewed lithospheric flexure. The graben density in each concentric band increases with the increase in band radius, inferring an increase in surface stress primarily at the forebulge. This increase in forebulge prominence can imply influences

from the increase in edifice mass, a shallower magma chamber as time progresses, as discussed above, or a decreasing T_e , possibly due to lithospheric thinning. Using some conclusions from Grosfils (2007), Hurwitz et al. (2009), Galgana et al. (2011), and Galgana et al. et al. (2013) we suggest the concentric graben bands about EM could record cycles of radial dike formation with sufficient elapsed time between these events to permit lithospheric flexure, where the increase in graben density in each graben band with increasing radius not only implies increase in edifice mass but could also infer magma chamber shallowing or lithospheric erosion as time progressed.

We now consider the disposition of the matching channels, which are more distally located from the EM caldera than many other features mapped in the study area. It has been suggested earlier these channels were originally the output from eccentric dikes (Allcocella et al., 2002) produced after the restrictions of the main conduit flow, so diverting magma radially. The up slope development of eccentric dikes has not been explained, however they have been associated with slopes and edifice instability (Allcocella et al., 2002). An alternative hypothesis could attribute province growth as a control of channel head ward development., both Hurtwitz (2009) and Galgana (2013) predict radial magma flow on the edifice-lithosphere boundary. This boundary would have a tendency to move upslope as the province grew due to growth of volcanic deposition and increase in uplift. The channels crosscut the recent flank flows implying late stage activity however the sequential nature of the measured channel changes and its linkage to the graben cross cutting sequence infers these channels contemporaneously developed overtime and started with only the Province basement in place and before any volcanic activity. In summary the matching channels have been active throughout the graben creation phases and have reflected changes in regional stress by variations by their channel axis direction changes. It is possible that all channels first developed as rilles and later, after the volcanic activity subsided, ephemeral supplies of water created an environment for selective mass wasting converting some rilles, or parts of them, into theater headed channel morphology.

We summarize the progression and possible sources of tectonic influence during channel development in Fig 11 where the possible event sources influencing channel directions are shown. We constrained the channel development timescales using our regional stress sequence reconciled with volcanic activity estimates based on crater counting (Platz and Michael, 2001 and Werner, 2009 and Robbins et al., 2011.. We have argued the NWSE graben are not likely to be the product of Tharsis Montes related flexure but possibly regional uplift. The correspondence between plume related uplift and volcanism is consistent with our development sequence, since after the formation of the NWSE graben the HT and EM edifices are developed. The NWSE graben development influenced the first two stages of channel growth (Fig 11(a) and Fig 11 (b)). There is a distinct change in channel azimuth between Fig 11(a) and Fig 11(b) however graben clustering is less distinctive. The development of HT preceded EM but there is no evidence of this event influencing the growth of EM, rather the converse, where EM development possibly limited the growth of HT. We suggest during EM stratocone development radial dike formations occurred which we initially categorized these as HT graben, and these are shown as stages 3, 4 and 5 in Fig 11. SER is shown as stage 6 in Fig 11 however we have been unable to affiliate this group with an event or tectonic feature. From the number of discrete sets of concentric EM graben rings (possibly 5) there are several intervals where sufficient time delay has occurred in EM edifice mass

accretion for lithospheric flexure and forebulge development to occur. The increase in EM concentric graben density with increase in radius provides possible indications of edifice mass increase, magma chamber shallowing or lithospheric thinning. The delays inferred between concentric graben clusters could imply cycles of main conduit blockage halting edifice growth (Galgana et al. 2013) and radial graben creation. The growth of HT prior to EM is consistent with the sequence proposed by Robbins et al. (2011) however this does not exclude lower levels of activity of HT continuing into the late Amazonian (Werner, 2009 and Robbins et al., 2011). AT has been considered as flank volcano and its size has excluded it from consideration, and the tectonic influence of HT on Province development has not been evident from the study.

An observation worthy of note is the unique disposition and number of similar channels within the study area in comparison the remainder of the Province. The larger channels are mutually parallel and enclosed by the northwesterly projections of the N and S bands of, the NWSE graben. These large channels have their longitudinal development to the NW relatively unconstrained as they discharged into the Utopia Planitia Basin (Thomson et al. 2001). The relationship between the channels, the regional topography, and the impact of the Utopia Basin on the development of the Province western flank of this beyond the scope of this study.

8 Conclusion

We have demonstrated: 1) graben are systematically arranged around sources of lithospheric loading and tectonic stress; 2) there is a correlation between the graben crosscutting sequence, channel direction and tectonic control and ; 3) from cross cutting analysis we have determined a common sequence of stress events across the study area implying a regional development sequence of volcanic and tectonic activity

Our approach to the analysis has been novel and we have been able to provide accurate data for the support of our propositions. We understand this is the first time the temporal sequence of tectonic, volcanic and channel evolution for the northwestern region of this major magmatic province on Mars has been proposed, using data which is independent of crater dating techniques.

9 Acknowledgements

The standard data used in this study are available at the NASA PDS Imaging Node, Mars Reconnaissance Orbiter Online Data Volumes (<https://pdsimaging.jpl.nasa.gov/volumes/mro.html>). The DTM used is available through https://astrogeology.usgs.gov/search/map/Mars/Topography/HRSC_MOLA_Blend/Mars_HRSC_MOLA_Blend_DEM_Global_200mpdata. Additional information and some intermediate data is provided in the supplementary information provided with the paper. We thank Professor Hauck II and the anonymous reviewers for helpful comments that improved the quality of this paper. The investigation is self-funded by B D Kneller.

10 References

- Alber, A., Piégay, H. (2011). Spatial disaggregation and aggregation procedures for characterizing fluvial features at the network-scale: Application to the Rhône basin (France). *Geomorphology*, 125(3), 343-360.
- Acocella, V. and Neri, M., 2003. What makes flank eruptions? The 2001 Etna eruption and its possible triggering mechanisms. *Bulletin of Volcanology*, 65(7), pp.517-529.
- Banerdt, W.B., Phillips, R.J., Sleep, N.H. & Saunders, R.S. (1982). Thick shell tectonics on one-plate planets: Applications to Mars. *Journal of Geophysical Research: Solid Earth*, 87(B12), 9723-9733.
- Belleguic, V., Lognonné, P. and Wieczorek, M. (2005). Constraints on the Martian lithosphere from gravity and topography data. *Journal of Geophysical Research: Planets*, 110(E11).
- Bistacchi, A., Tibaldi, A., and Rust, D., 2012. A new model for cone sheet emplacement: data from the Isle of Skye (UK) and numerical modeling. *Earth and Planetary Science Letters*, 339(340), pp.46-56.
- Bonforte, A., Gambino, S. and Neri, M., 2009. Intrusion of eccentric dikes: the case of the 2001 eruption and its role in the dynamics of Mt. Etna volcano. *Tectonophysics*, 471(1-2), pp.78-86.
- Carr, M.H., Clow, G.D. (1981). Martian channels and valleys: Their characteristics, distribution, and age. *Icarus*, 48(1), 91-117.
- Clifford, S.M. (1993). A model for the hydrologic and climatic behavior of water on Mars. *Journal of Geophysical Research: Planets*, 98(E6), 10973-11016.
- Chen, Y., Gupta, M.R. (2010). EM demystified: An expectation-maximization tutorial. *Electrical Engineering*.
- Christiansen, E.H. (1989). Lahars in the Elysium region of Mars. *Geology*, 17(3), 203-206.
- Christensen, P.R., Jakosky, B.M., Kieffer, H.H., Malin, M.C., McSween, H.Y., Neelson, K., Mehall, G.L., Silverman, S.H., Ferry, S., Caplinger, M. and Ravine, M. (2004). The thermal emission imaging system (THEMIS) for the Mars 2001 Odyssey Mission. *Space Science Reviews*, 110(1-2), 85-130.
- Comer, R.P., Solomon, S.C. and Head, J.W. (1985). Mars: Thickness of the lithosphere from the tectonic response to volcanic loads. *Reviews of Geophysics*, 23(1), 61-92.
- Criel, J., Tsiorkova, E. (2005). Gene Time Expression Warper: a tool for alignment, template matching and visualization of gene expression time series. *Bioinformatics*, 22(2), 251-252.

Delamere, W.A., Tornabene, L.L., McEwen, A.S., Becker, K., Bergstrom, J.W., Bridges, N.T., Eliason, E.M.,
Gallagher, D., Herkenhoff, K.E., Keszthelyi, L. and Mattson, S., 2010. Color imaging of Mars by the High
Resolution Imaging Science Experiment (HiRISE). *Icarus*, 205(1), 38-52.

Do, C.B., Batzoglou, S. (2008). What is the expectation maximization algorithm? *Nature biotechnology*, 26(8),
897-899.

Ernst, R.E., Head, J.W., Parfitt, E., Grosfils, E. and Wilson, L. (1995). Giant radiating dike swarms on Earth and
Venus. *Earth-Science Reviews*, 39(1-2), 1-58.

Ernst, R.E., Grosfils, E.B. and Mege, D. (2001). Giant dike swarms: Earth, Venus, and mars. *Annual Review of
Earth and Planetary Sciences*, 29(1), 489-534.

Ferrill, D.A. and Morris, A.P. (2003). Dilational normal faults. *Journal of Structural Geology*, 25(2), 183-196.

Fraley, C. and Raftery, A.E. (2002). Model-based clustering, discriminant analysis, and density estimation.
Journal of the American statistical Association, 97(458), 611-631.

Fraley, C. and Raftery, A.E. (2006). "MCLUST" version 3: an R package for normal mixture modeling and
model-based clustering. *Washington University, Seattle , Department of Statistics*.

Geshi, N., 2008. Vertical and lateral propagation of radial dikes inferred from the flow-direction analysis of the
radial dike swarm in Komochi Volcano, Central Japan. *Journal of Volcanology and Geothermal Research*,
173(1-2), pp.122-134.

Giorgino, T. (2009). Computing and visualizing dynamic time warping alignments in R: the "dtw" package.
Journal of statistical Software, 31(7), pp.1-24.

Gornitz, V. (1973). The origin of sinuous rilles. *The moon*, 6(3-4), pp.337-356.

Greeley, R., Spudis, P.D. (1981). Volcanism on Mars. *Reviews of Geophysics*, 19(1), 13-41.

Grosfils, E.B., 2007. Magma reservoir failure on the terrestrial planets: Assessing the importance of
gravitational loading in simple elastic models. *Journal of Volcanology and Geothermal Research*, 166(2),
pp.47-75.

Galgana, G.A., McGovern, P.J. and Grosfils, E.B., 2011. Evolution of large Venusian volcanoes: Insights from
coupled models of lithospheric flexure and magma reservoir pressurization. *Journal of Geophysical Research:
Planets*, 116(E3)

1161
1162
1163
1164
1165
1166
1167
1168
1169
1170
1171
1172
1173
1174
1175
1176
1177
1178
1179
1180
1181
1182
1183
1184
1185
1186
1187
1188
1189
1190
1191
1192
1193
1194
1195
1196
1197
1198
1199
1200

Galgana, G.A., Grosfils, E.B. and McGovern, P.J., 2013. Radial dike formation on Venus: Insights from models of uplift, flexure and magmatism. *Icarus*, 225(1), pp.538-547.

Golombek M. (1989). A Review of extensional tectonic features on Mars, *Tectonic Features on Mars* 33-35

Gulick, V.C. (2001). Origin of the valley networks on Mars: A hydrological perspective. *Geomorphology*, 37(3), 241-268.

Hall, J.L., Solomon, S.C. and Head, J.W. (1986). Elysium region, Mars: Tests of lithospheric loading models for the formation of tectonic features. *Journal of Geophysical Research: Solid Earth*, 91(B11), 11377-11392.

Hartmann, W.K. and Neukum, G. (2001). Cratering chronology and the evolution of Mars. *Space Science Reviews*, 96(1), 165-19.

Hartmann, W.K. (2005). Martian cratering 8: Isochron refinement and the chronology of Mars. *Icarus*, 174(2), 294-320.

Head III, J.W. and Wilson, L., 1993. Lunar graben formation due to near-surface deformation accompanying dike emplacement. *Planetary and Space Science*, 41(10), pp.719-727.

Howard, A.D., Moore, J.M. and Irwin, R.P., (2005). An intense terminal epoch of widespread fluvial activity on early Mars: 1. Valley network incision and associated deposits. *Journal of Geophysical Research: Planets*, 110(E12).

Hurwitz, D.M., Long, S.M. and Grosfils, E.B., 2009. The characteristics of magma reservoir failure beneath a volcanic edifice. *Journal of Volcanology and Geothermal Research*, 188(4), pp.379-394.

Hurwitz, D.M., Head, J.W. and Hiesinger, H., (2013). Lunar sinuous rilles: Distribution, characteristics, and implications for their origin. *Planetary and Space Science*, 79, 1-38.

Hynek, B.M., Beach, M. and Hoke, M.R. (2010). Updated global map of Martian valley networks and implications for climate and hydrologic processes. *Journal of Geophysical Research: Planets*, 115(E9)

Jaeger, W.L., Keszthelyi, L.P., Skinner Jr, J.A., Milazzo, M.P., McEwen, A.S., Titus, T.N., Rosiek, M.R., Galuszka, D.M., Howington-Kraus, E. and Kirk, R.L., 2010. Emplacement of the youngest flood lava on Mars: A short, turbulent story. *Icarus*, 205(1), pp.230-243.

Janle, P., Ropers, J. (1983). Investigation of the isostatic state of the Elysium dome on Mars by gravity models, *In Physics of the Earth and Planetary Interiors*, Volume 32, Issue 2, 132-145.

1201

1202 Keogh, E.J. and Pazzani, M.J. (2001). Derivative dynamic time warping. In *Proceedings of the 2001 SIAM*
1203 *International Conference on Data Mining* (pp. 1-11). Society for Industrial and Applied Mathematics.

1204

1205 Lamb, M.P., Howard, A.D., Johnson, J., Whipple, K.X., Dietrich, W.E. and Perron, J.T. (2006). Can springs cut
1206 canyons into rock?. *Journal of Geophysical Research: Planets*, 111(E7).

1207

1208 Lamb, M.P., Mackey, B.H. and Farley, K.A. (2014). Amphitheater-headed canyons formed by megaflooding at
1209 Malad Gorge, Idaho. *Proceedings of the National Academy of Sciences*, 111(1), 57-62.

1210

1211 Laity, J.E. and Malin, M.C. (1985). Sapping processes and the development of theatre-headed valley networks
1212 on the Colorado Plateau. *Geological Society of America Bulletin*, 96(2), 203-217.

1213

1214 Laity, J.E. (1990). Spring sapping and valley network development. *Groundwater Geomorphology: The role of*
1215 *subsurface water in earth-surface processes and landforms*, Geological Society of America 252, 235 - 244.

1216

1217 Leverington, D.W. (2011). A volcanic origin for the outflow channels of Mars: Key evidence and major
1218 implications. *Geomorphology*, 132(3), 51-75.

1219

1220 Madeleine, J.B., Forget, F., Head, J.W., Levrard, B., Montmessin, F. and Millour, E. (2009). Amazonian
1221 northern mid-latitude glaciation on Mars: A proposed climate scenario. *Icarus*, 203(2), 390-405.

1222

1223 Malin, M.C., Bell, J.F., Cantor, B.A., Caplinger, M.A., Calvin, W.M., Clancy, R.T., Edgett, K.S., Edwards, L.,
1224 Haberle, R.M., James, P.B. and Lee, S.W. (2007). Context camera investigation on board the Mars
1225 Reconnaissance Orbiter. *Journal of Geophysical Research: Planets*, 112(E5).

1226

1227 MacKinnon, D.J. and Tanaka, K.L. (1989). The impacted Martian crust: Structure, hydrology, and some
1228 geologic implications. *Journal of Geophysical Research: Solid Earth*, 94(B12), 17359-17370

1229 .

1230 McGovern, P.J., Solomon, S.C., Smith, D.E., Zuber, M.T., Simons, M., Wieczorek, M.A., Phillips, R.J.,
1231 Neumann, G.A., Aharonson, O. and Head, J.W. (2002). Localized gravity/topography admittance and
1232 correlation spectra on Mars: Implications for regional and global evolution. *Journal of Geophysical Research:*
1233 *Planets*, 107(E12).

1234

1235 McKenzie, D., Barnett, D.N. and Yuan, D.N. (2002). The relationship between Martian gravity and topography.
1236 *Earth and Planetary Science Letters*, 195(1), 1-16.

1237

1238 Neukum, G. and Jaumann, R. (2004). HRSC: The high resolution stereo camera of Mars Express. In *Mars*
1239 *Express: The Scientific Payload* (Vol. 1240), 17-35.

1240

- Pedersen, G.B.M., Head, J.W. and Wilson, L., 2010. Formation, erosion and exposure of Early Amazonian dikes, dike swarms and possible subglacial eruptions in the Elysium Rise/Utopia Basin Region, Mars. *Earth and Planetary Science Letters*, 294(3), 424-439.
- Platz, T. and Michael, G. (2011). Eruption history of the Elysium volcanic province, Mars. *Earth and Planetary Science Letters*, 312(1), 140-151.
- Rabiner, L.R. and Juang, B.H. (2008). Fundamentals of speech recognition. Published by Pearson India (2008) ISBN 10: [8177585606](#), ISBN 13: [9788177585605](#)
- Rath, T.M. and Manmatha, R. (2003). Word image matching using dynamic time warping. In *Computer Vision and Pattern Recognition, 2003. Proceedings. 2003 IEEE Computer Society Conference on* (Vol. 2, pp. II-II). IEEE.
- Robbins, S.J., Di Achille, G. and Hynek, B.M. (2011). The volcanic history of Mars: High-resolution crater-based studies of the calderas of 20 volcanoes. *Icarus*, 211(2), 1179-1203.
- Roux, C., Alber, A., Piégay, H., 2013. Centerline guideline for the *FluvialCorridor* toolbox, a new ArcGIS toolbox package for exploring multiscale riverscape at a network scale. Sedalp (Sediment Management in Alpine Basins) and CNRS (UMR5600).
- Roux, C., Alber, A., and Bertrand, M., Vaudor, L. and Piégay, H. (2015). “FluvialCorridor”: A new ArcGIS toolbox package for multiscale riverscape exploration. *Geomorphology*, 242, 29-37.
- Russell, P.S. and Head, J.W. (2003). Elysium-Utopia flows as mega-lahars: A model of dike intrusion, cryosphere cracking, and water-sediment release. *Journal of Geophysical Research: Planets*, 108(E6).
- Sakoe, H. and Chiba, S., 1978. Dynamic programming algorithm optimization for spoken word recognition. *IEEE transactions on acoustics, speech, and signal processing*, 26(1), pp.43-49.
- Sakoe, H. and Chiba, S., 1978. Dynamic programming algorithm optimization for spoken word recognition. *IEEE transactions on acoustics, speech, and signal*
- Schultz, R.A., Moore, J.M., Grosfils, E.B., Tanaka, K.L. and Mege, D., 2007. The Canyonlands model for planetary grabens: Revised physical basis and implications. *The Geology of Mars: Evidence from Earth-Based Analogs*, pp.371-399.
- Solomon, S.C. and Head, J.W., 1980. Lunar mascon basins: Lava filling, tectonics, and evolution of the lithosphere. *Reviews of Geophysics*, 18(1), pp.107-141.
- Tanaka, K.L., Chapman, M.G. and Scott, D.H. (1992). Geologic map of the Elysium region of Mars (No. 2147).

- Tanaka, K.L. and Golombek, M.P. (1989). Martian tension fractures and the formation of grabens and collapse features at Valles Marineris. In *Lunar and Planetary Science Conference Proceedings* (Vol. 19), 383-396.
- Tanaka, K.L., Skinner, J.A. and Hare, T.M. (2005). Geologic map of the northern plains of Mars. *USGS Scientific Investigations Map* 2888.
- Tanaka, K.L., Skinner Jr, J.A., Dohm, J.M., Irwin III, R.P., Kolb, E.J., Fortezzo, C.M., Platz, T., Michael, G.G. and Hare, T.M. (2014). Geologic Map of Mars, *USGS Scientific Investigations Map* 3292.
- Thomson, B.J. and Head III, J.W., 2001. Utopia Basin, Mars: Characterization of topography and morphology and assessment of the origin and evolution of basin internal structure. *Journal of Geophysical Research: Planets*, 106(E10), pp.23209-23230.
- Tormene, P., Giorgino, T., Quaglini, S. and Stefanelli, M., 2009. Matching incomplete time series with dynamic time warping: an algorithm and an application to post-stroke rehabilitation. *Artificial intelligence in medicine*, 45(1), pp.11-34.
- Wang, C.P. and Isenhour, T.L. (1987). Time-warping algorithm applied to chromatographic peak matching gas chromatography/Fourier transform infrared/mass spectrometry. *Analytical Chemistry*, 59(4), 649-654.
- Werner, S.C. (2009). The global Martian volcanic evolutionary history. *Icarus*, 201(1), 44-68.
- Wilson, L. and Mouginis-Mark, P. (1984). Martian sinuous rilles. *Lunar and Planetary Science Conference* (Vol. 15), 926-927.
- Wyrick, D., Ferrill, D.A., Morris, A.P., Colton, S.L. and Sims, D.W. (2004). Distribution, morphology, and origins of Martian pit crater chains. *Journal of Geophysical Research: Planets*, 109(E6).

Figure Captions

Fig.1. An overview of the channel locations, their regional, stratigraphic and lithospheric stress distributions. (a) The study area channel locations showing their relative positions on the Elysium Rise, and the channel direction changes in channels 1&2 that were initially observed. (b) An indication of the regional graben distribution, and the location of the study area in the NW quadrant within the Elysium Province. The regional NW to SE graben (dark brown) are shown mostly in the NW and SE quadrant. (c) An adaptation of Hall 1986 Fig 12 showing the lithospheric stress distribution within the region by assuming loading from Tharsis Montes, Elysium Mons and Hecates Tholus. Also included were the influences of plume activity and regional uplift. (d) Regional geology

(Tanaka, 2014) where Hve – Hesperian volcanic units; AHv the younger Amazonian/Hesperian volcanic units; IHvf a late Hesperian volcanic field.

Fig 2: The initial evaluation of the spatial and azimuthal dependence of mapped graben (342 samples). (a) the locations of mapped graben. (b) The population probability density function showing multiple modes M1 to M5. (c) Each mode was individually selected using ArcGIS functionality and the graben members of each mode can be seen color matched with the mode selected. The average direction of each mode azimuth is shown in the table.

Fig. 3 Graben azimuth population Probability Density Function (PDF). (a) The PDF three distinct modes. (b) The PDF color coded showing the PDF components that align with identifiable surface features shown with a breakdown of their relative contributions summarized below. (c) Rose frequency diagram of the NWSE graben occurring in the SE quadrant. (d) Rose frequency diagram of the NWSE graben occurring in the NW quadrant. (e) Details of the lithospheric forebulge profile modeled by Comer(1985) for EM and (f) the lithospheric stress distribution for a Venusian volcano by Galgana (2013) using a finite element model. It is noted that the forebulge for either model occurs at a similar distance from the edifice periphery, which is approximates to the edifice radius.

Fig 4. Graben azimuth distribution. (a) Summary showing the association of graben with sources of dilatational stress and the graben physical clustering with respect to these sources, which are linear, arcuate or clustered. (b) A revised version of Hall et .al (1986) Fig 12 showing the stress field distributions predicted by them and their relationship with the Elysium Province topography. Equivalence can be seen between the study results (a) and the distributions in (b) though their relative positions can be different. The study area is marked as grey shading in (b),

Fig 5. Study Area Crosscutting Relationships. (a) Crosscutting graben locations showing examples of the crosscutting images in the inset. (b) A summary of all crosscutting relationships showing the time ordered relationships and their locations. (c) The crosscutting relationships summarized from 5(b) showing the cross cutting time progression. (d) The cross cutting further summarized and expressed as changes in direction.

Fig 6 Channels 1, 2 and 8 Linear Reference Axes (LRA) and floor area polygons. (a),(c),(e) The LRA profile in graphic form showing the detailed variation in channel azimuth along their lengths. (b), (d), (f) The LRA is shown as red line in these images and floor area polygon in yellow. Channel 1, Figures (a) & (b), Channel 2 Figures (c) & (d), Channel 8 Figures (e) & (f) showing the section of profile used.

Fig 7. Channels 3,4,5,7 and 6 (in order). (a), (c), (e), (g), (i) The LRA in graphic form showing the detailed variation in channel azimuth along their lengths. (b), (d), (f), (h), (j) The LRA is shown as red line in these images and floor area polygon in orange. Showing Channel 3, Figures (a) & (b), Channel 4 Figures (c) & (d), Channel 5 Figures (e) & (f), Channel 7 (g) & (h) and Channel 6 (i) & (j).

Fig.8 Channel profile matching for Channels 1 and 2, and Channels 1 and 6. The initial profiles are normalized to 200 bins. The first column, the initial profile, shows plots of binned channel location (ordinate) and channel axis azimuth (abscissa). The second column, the post warped profiles, show both channel profiles after dynamic time warping and the regions where original profiles have been moved with respect to each other to achieve a match. In column three, a linear regression of the data, shows equivalent point alignment by warping providing a useful measure of correlation. The fourth column, the DTW standard 3way plot, shows the equivalent points and how they have been moved to achieve a match along the warping function. Channels 1 and 2 match along their complete lengths. The match between Channels 1 and 6 shows no match up to bin 90 Channel 6. Referring to Fig 8(i) and (j) the lack of matching excludes the lower section of the channel below the confluence at around bin 65 Channel 6. By implication the lower channel could be a separate development under different erosional conditions.

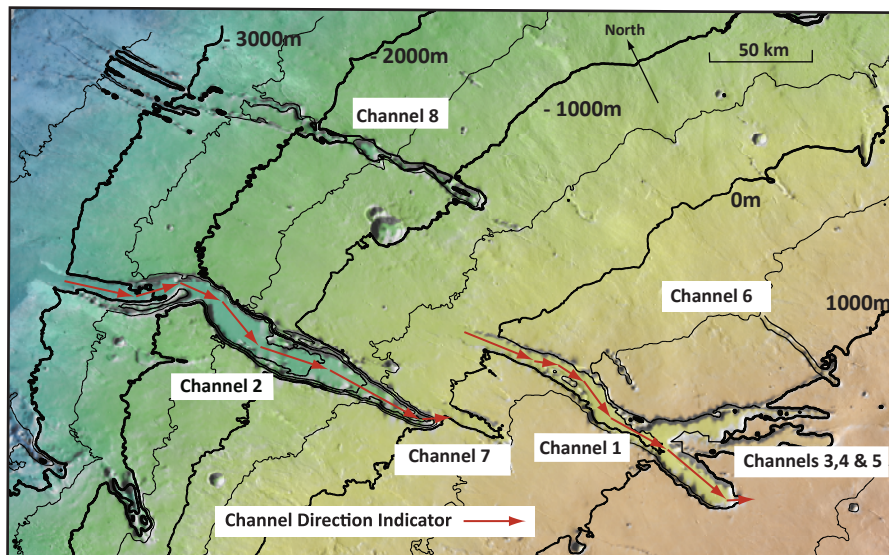
Fig 9 Channel profile matching for Channels 1 and 7, and Channels 1 and 8. The initial profiles are normalized to 200 bins. The first column, the initial profile, shows plots of binned channel location (ordinate) and channel axis azimuth (abscissa). The second column, the post warped profiles, show both channel profiles after dynamic time warping and the regions where original profiles have been moved with respect to each other to achieve a match. In column three, a linear regression of the data, shows equivalent point alignment by warping providing a useful measure of correlation. The fourth column, the DTW standard 3way plot, shows the equivalent points and how they have been moved to achieve a match along the warping function. Channel 1 and 7 match has many regions of inserted spaces and a major section of channel 1 profile has been shifted up axis to achieve a match. Only stages 1 and 2 are matched on a very few channel features (c and d). Channel 8 matches in the stages as shown even though Channels 1 and 8 morphologies are different.

Fig 10. Comparisons of Channels 1, 2, 6 and 8 showing equivalence in direction change along channel. (a) Changes in channel LRA (red line); the black arrows indicate the channel stage average azimuth; the yellow lines are the perpendiculars to each stage average azimuth indicating the possible direction of average dilatational stress. (b) Summarizes the changes in direction due to fault control assuming channel erosion migrated from mouth to head. (c) Summarizes the changes in direction due to fault control assuming channel erosion migrated from head to mouth. Diagrams (d) and (e)

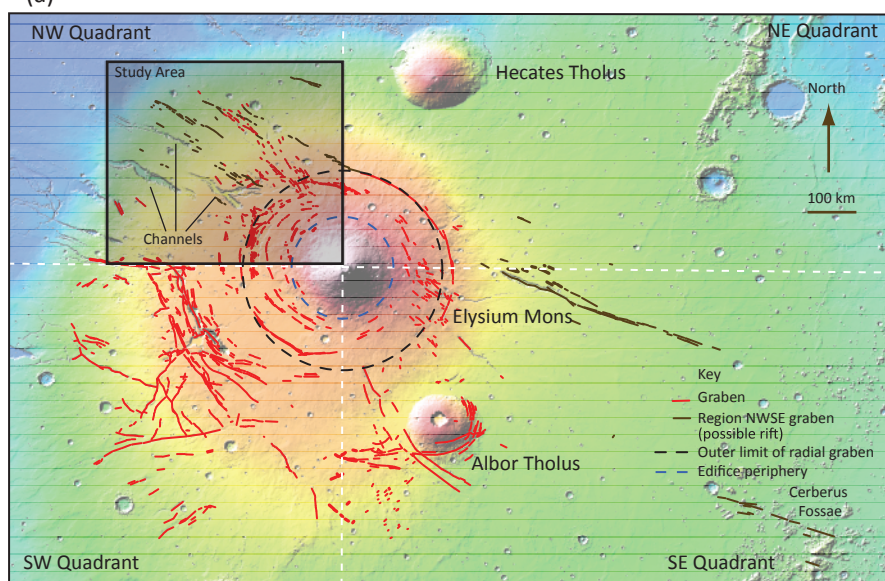
respectively summarize diagrams (b) and (c) by assuming a continuation of a general direction between channel stages can be consolidated e.g. stages 2 and 3 in 10(b).

Fig 11. The change of regional stress through time and its influence on channel development direction. We propose the extensional stress first acts on the channel mouth section and the changes in stress direction are shown stage by stage as the channel develops from mouth to channel head. We suggest the channel section shown in the window forms contemporaneously as the graben indicated in yellow are formed. Spatially defined subsets occur within the stage graben clusters and those graben not created in a particular stage are shown in red. For example in (c), (d) and (e) the sum of the red circles and yellow circles represent the total population of HT orientated graben in that cluster but only the yellow graben are being formed during the stages indicated.

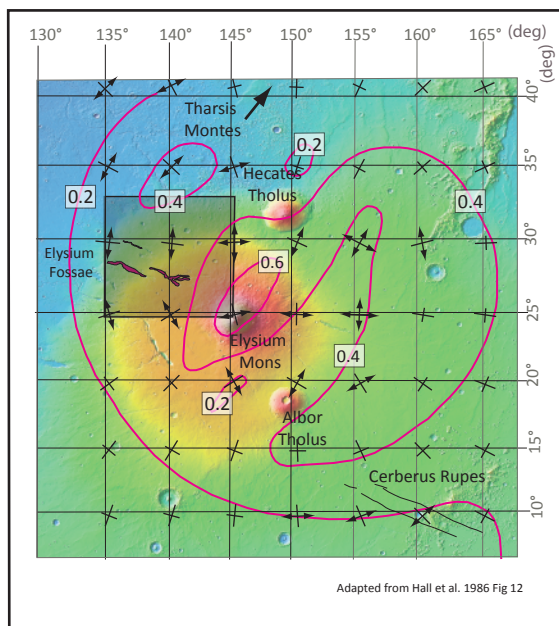
Figure 1.



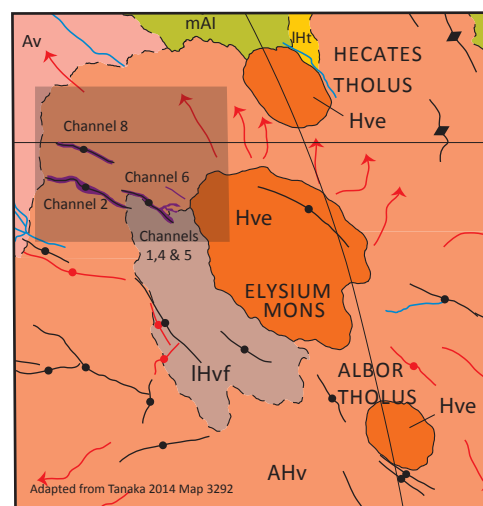
(a)



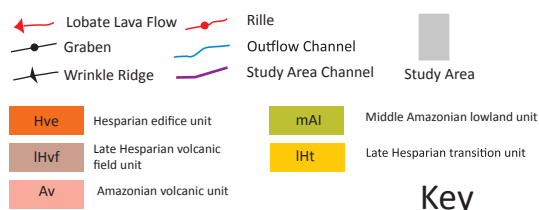
(b)



(c)

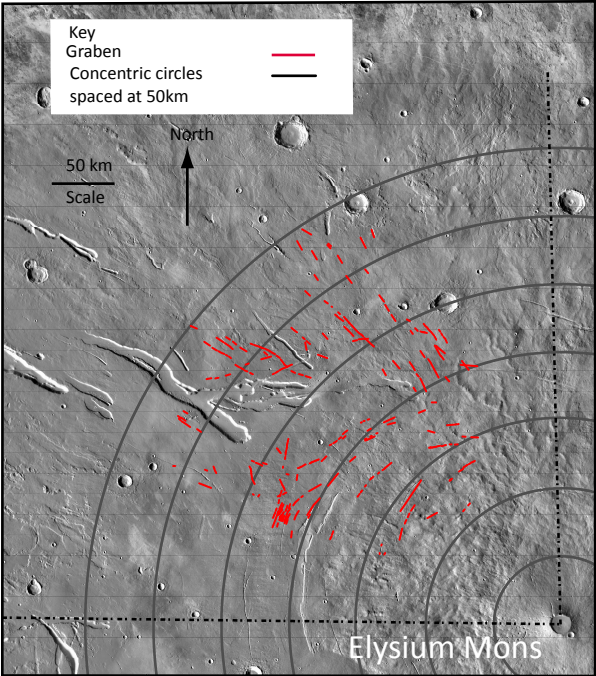


(d)

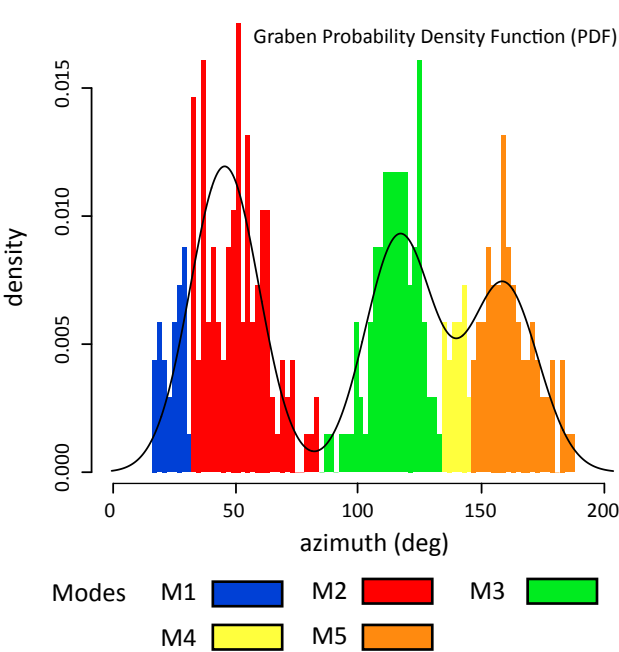


Key

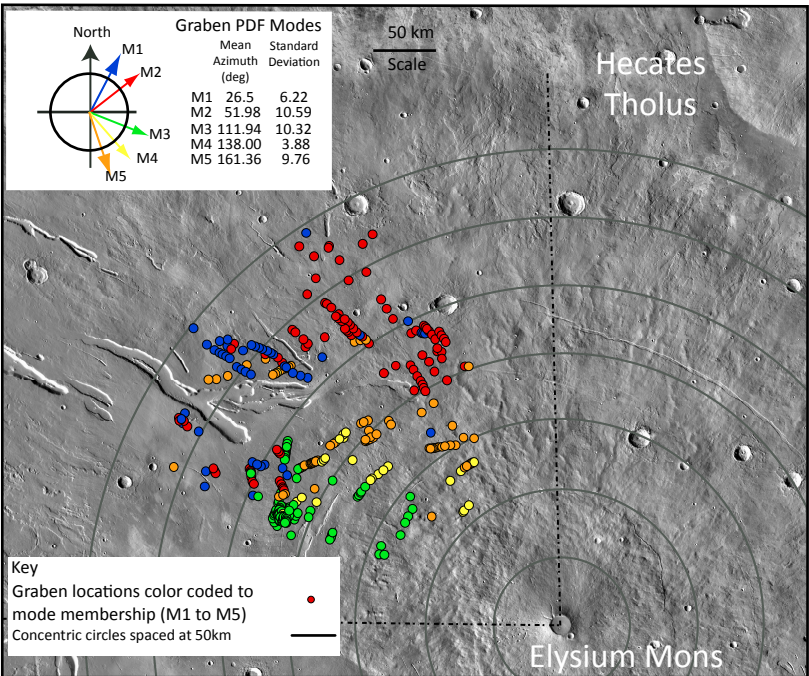
Figure 2.



(a)

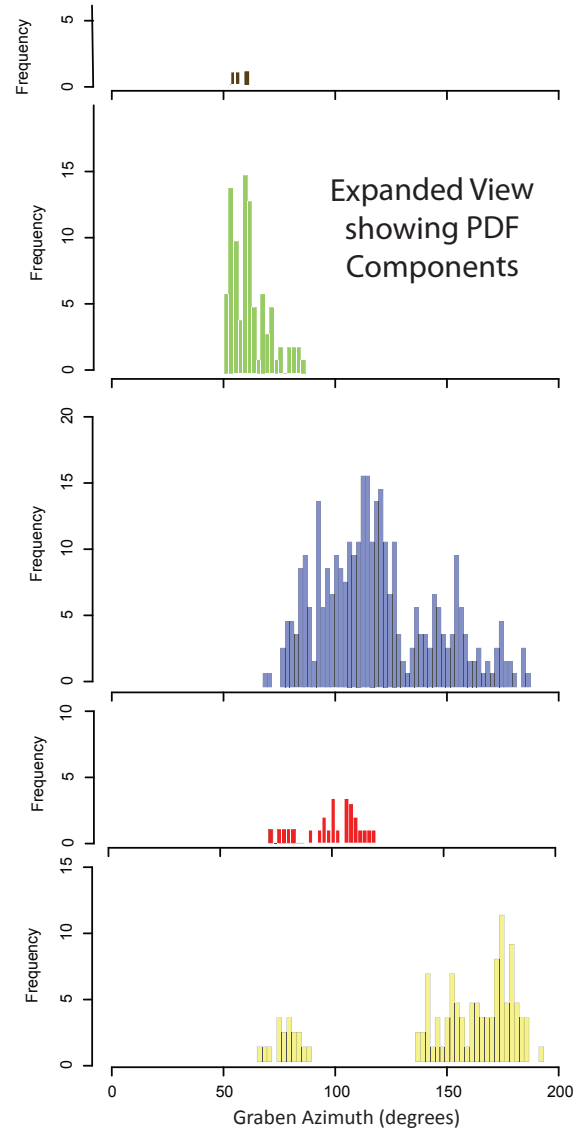
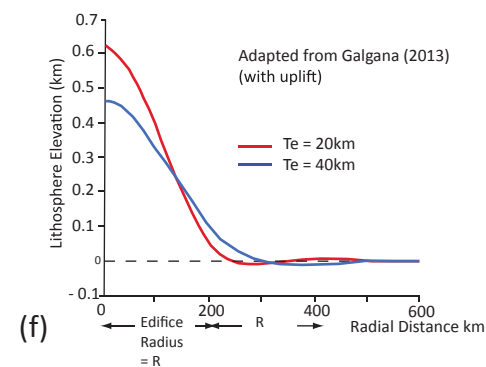
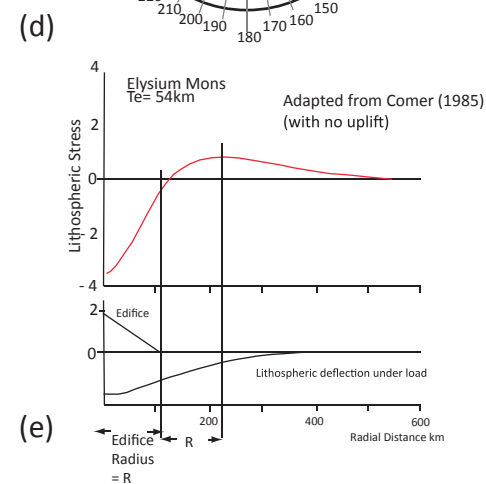
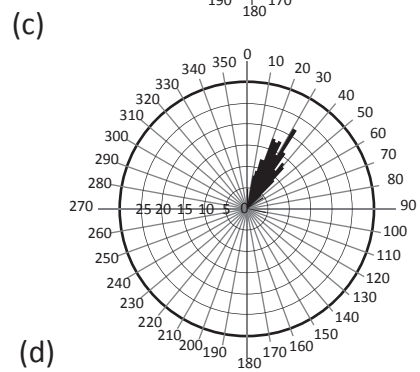
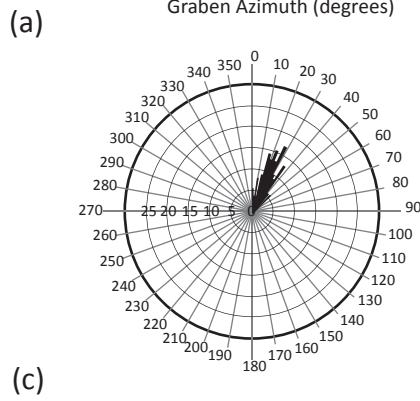
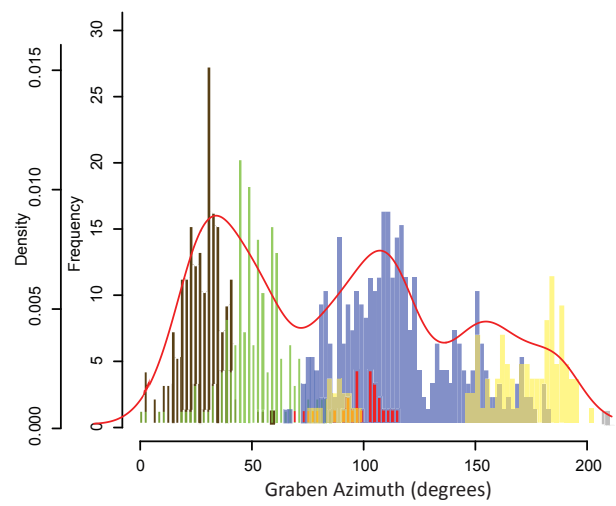
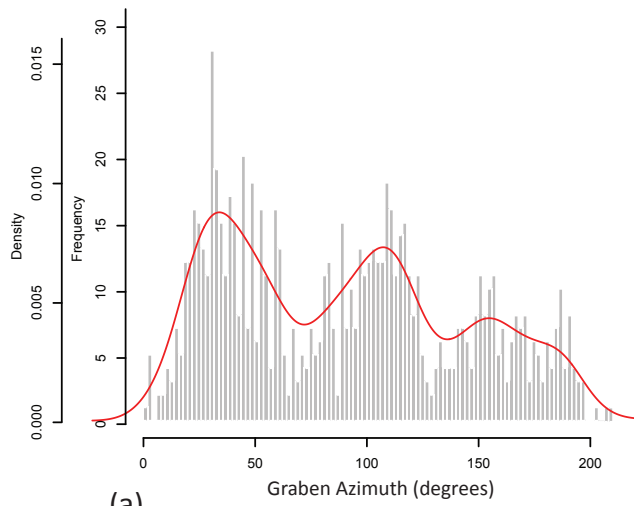


(b)



(c)

Figure 3.



(b)

Key

Hecates
Tholus (HT)

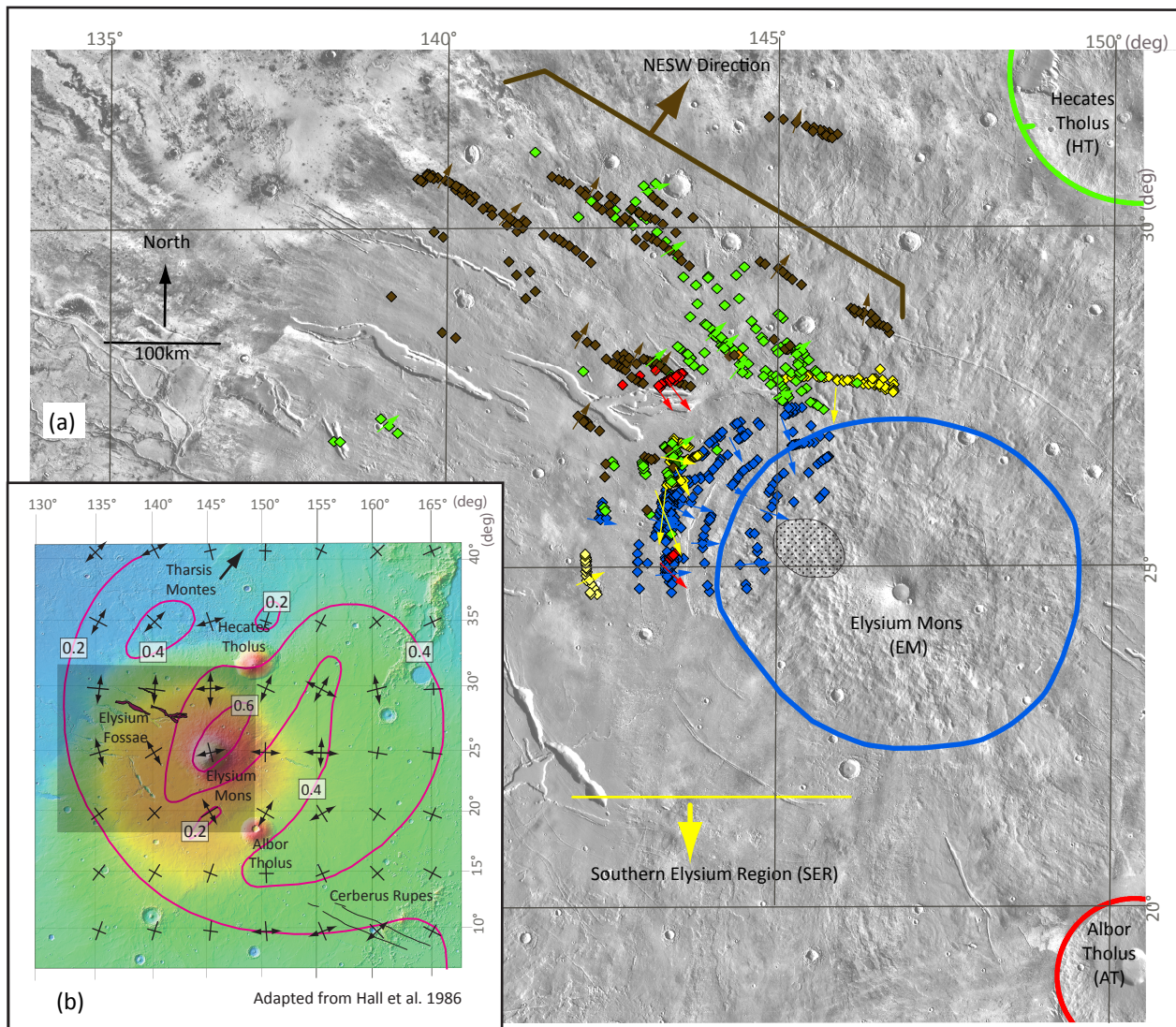
Albor
Tholus (AT)

Elysium
Mons (EM)

Southern
Elysium Rise (SER)

NW to SE
Graben bands (NWSE)

Figure 4.



Key

Graben direction color code

NWSE Hecates Elysium Albor Southern
 General Direction Tholus (HT) Mons (EM) Tholus (AT) Elysium Rise (SER)

Line of break in slope between the edifice indicated and the Elysium Rise.

HT ——— AT ——— EM ———

Study Area



Cluster Average

Azimuth. (Various Colours)

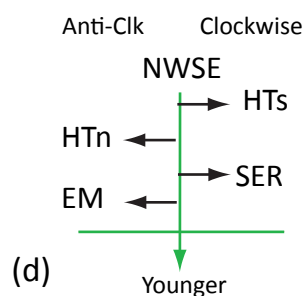
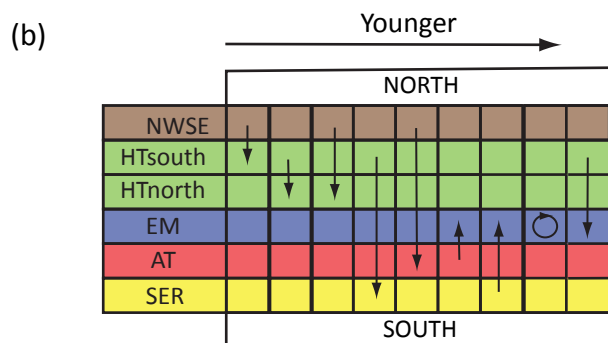
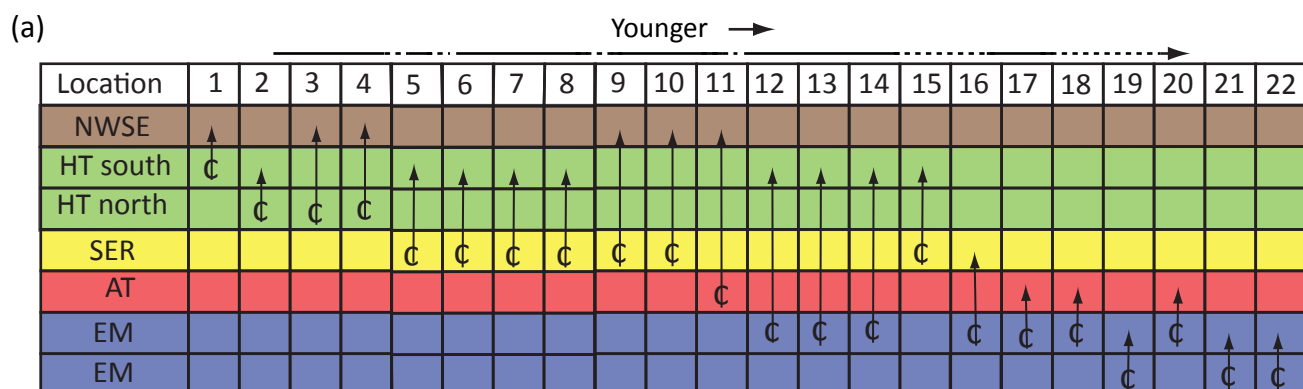
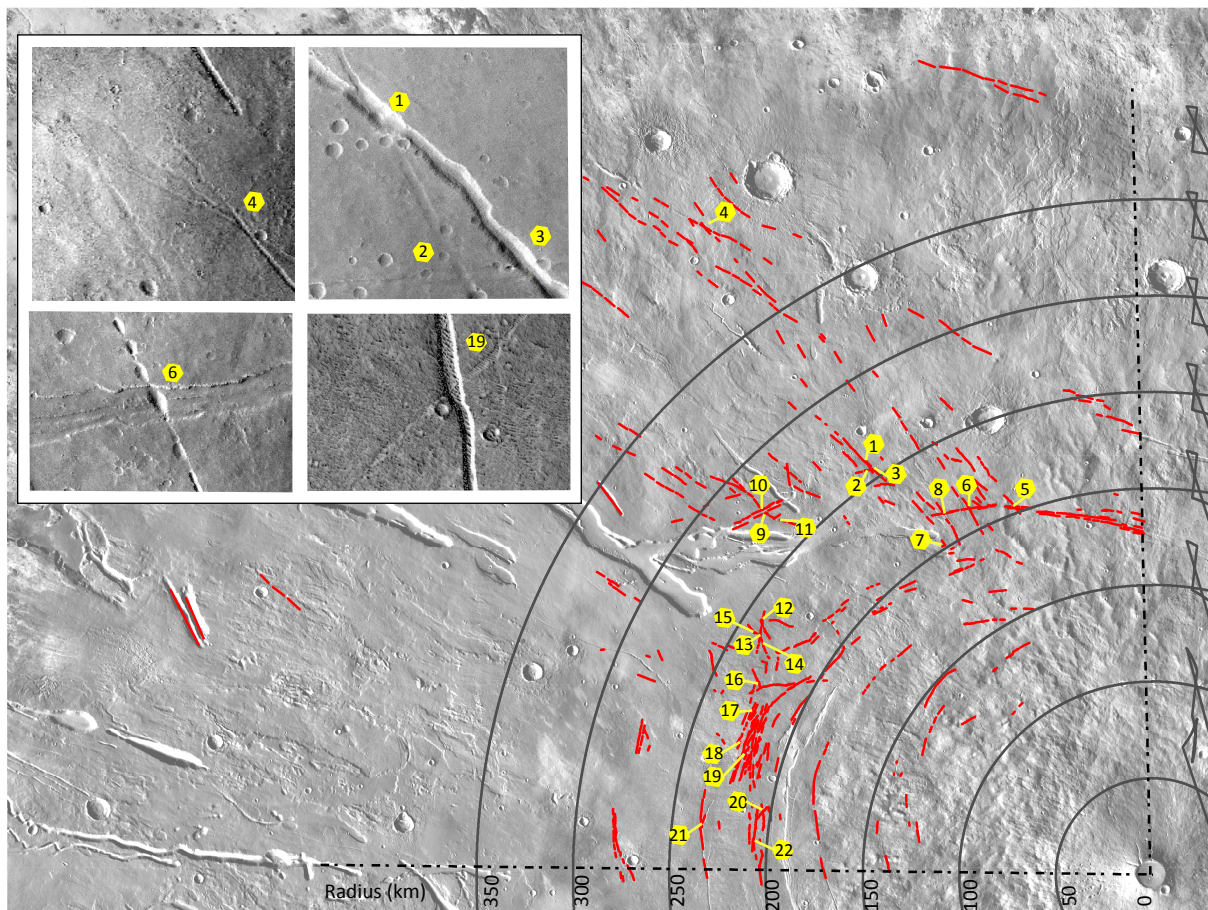


EM graben

convergence area



Figure 5.



- (c) **KEY**
- HTsouth ↻ NWSE = HTsouth crosscuts NWSE
- NESW = NESW graben bands
- HTnorth = Hecates Tholus - north side
- HTsouth = Hecates Tholus - south side
- EM = Elysium Mons

- AT = Albor Tholus
- SER = Southern Elysium Region
- > = Features getting younger
- dashed lines = uncertainty in progression due to separation

Figure 6.

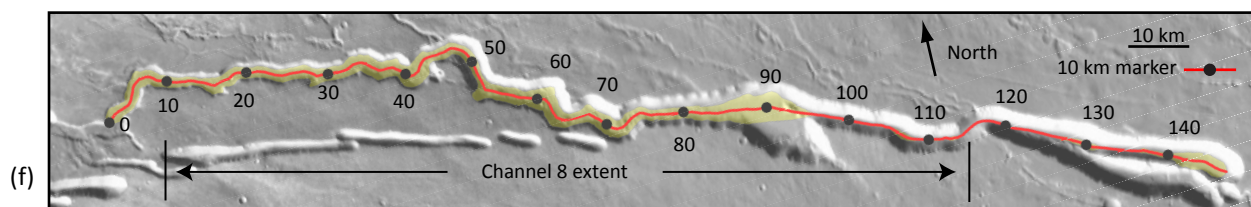
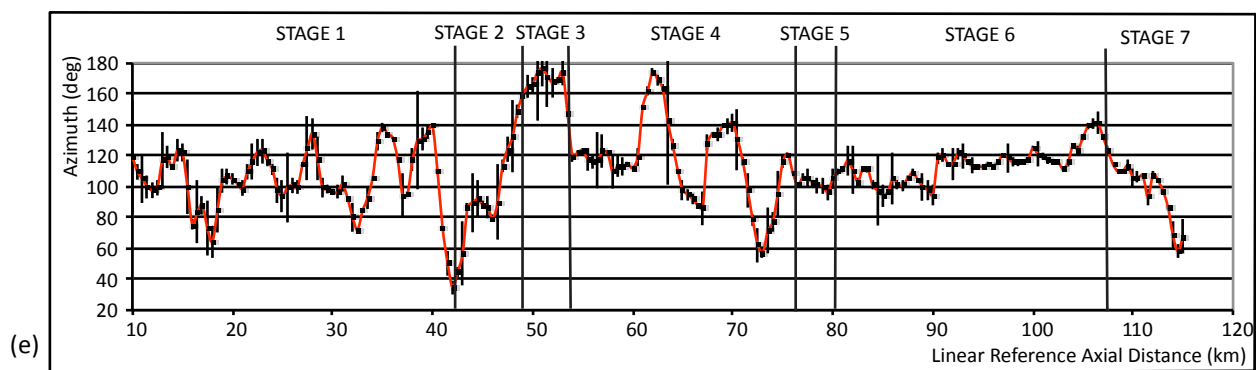
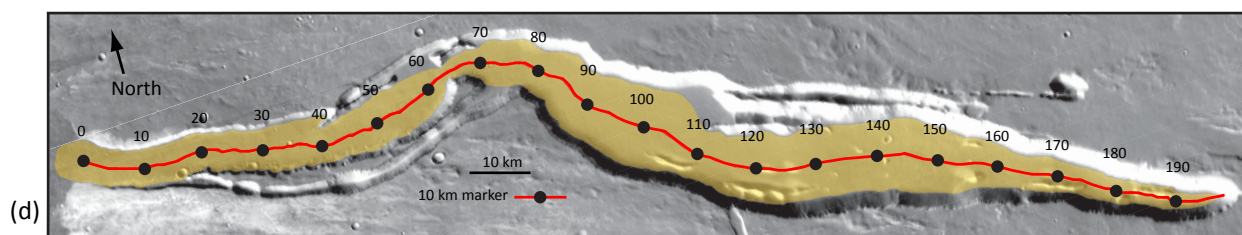
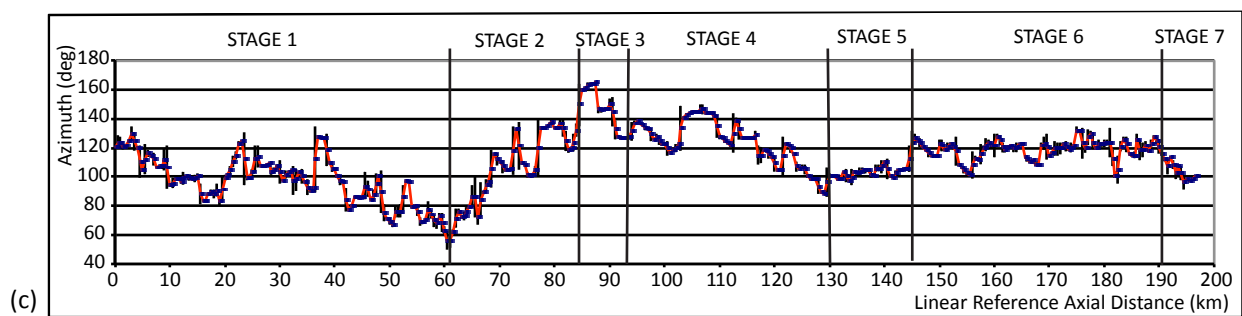
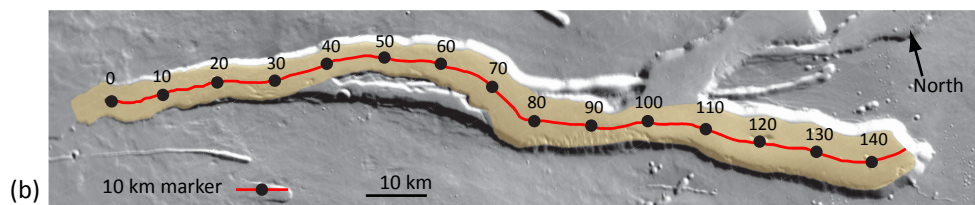
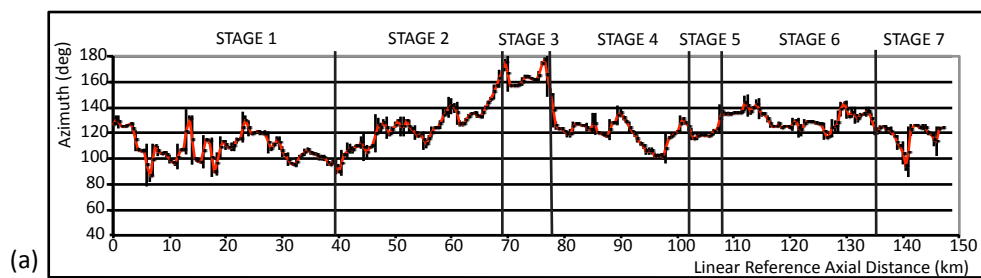


Figure 7.

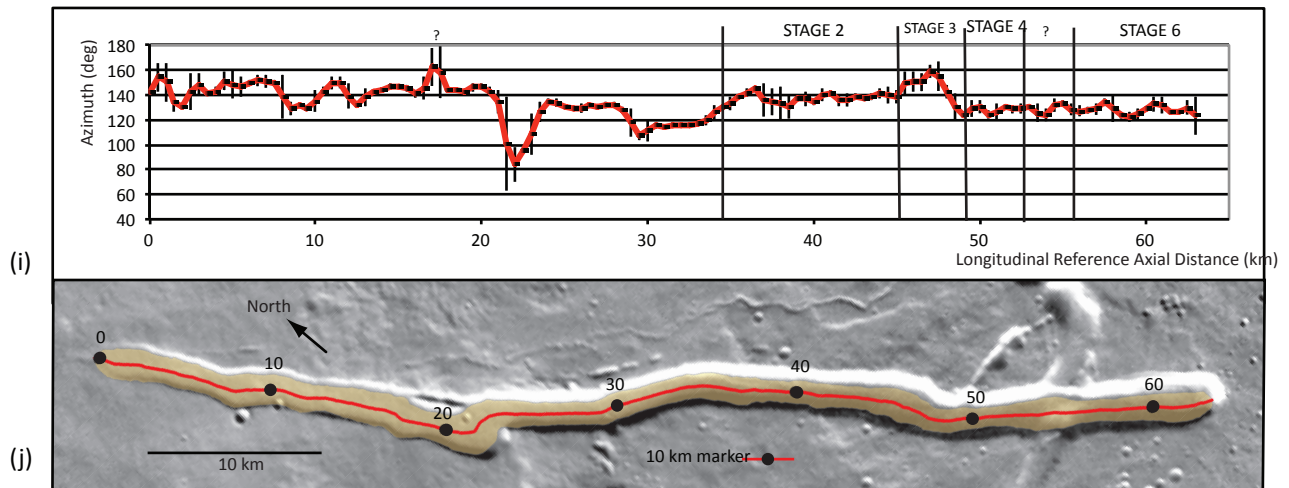
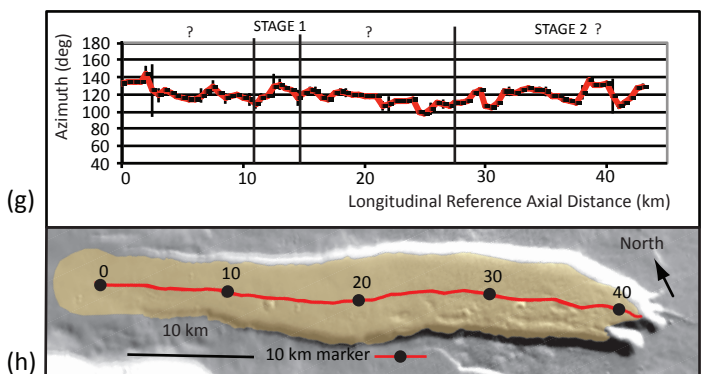
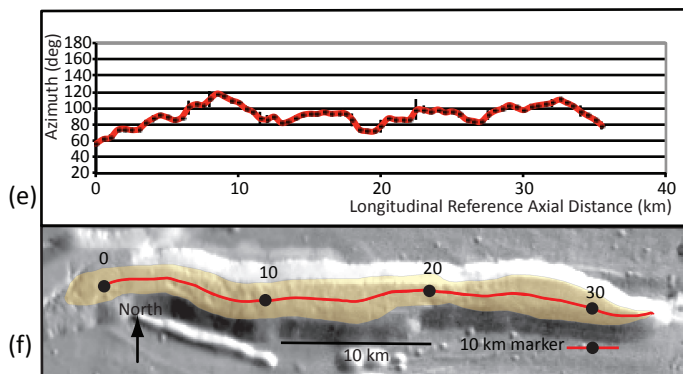
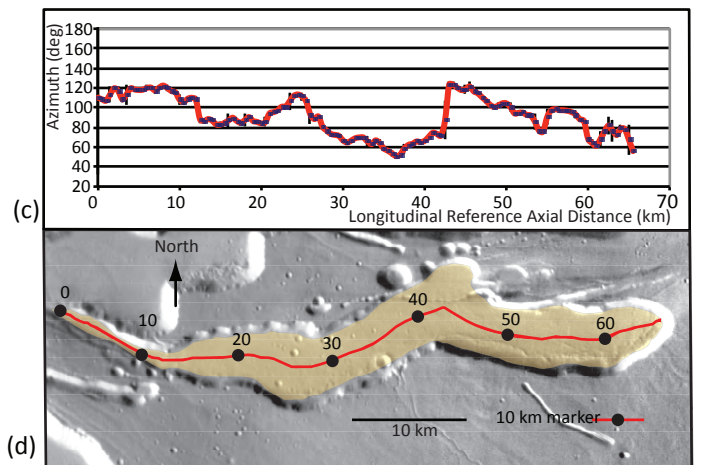
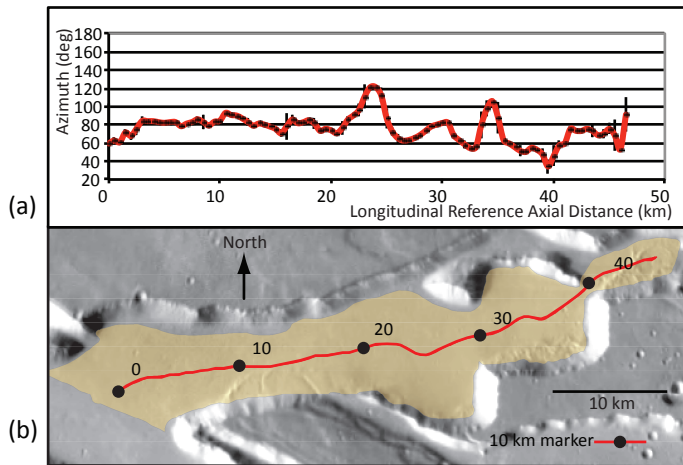
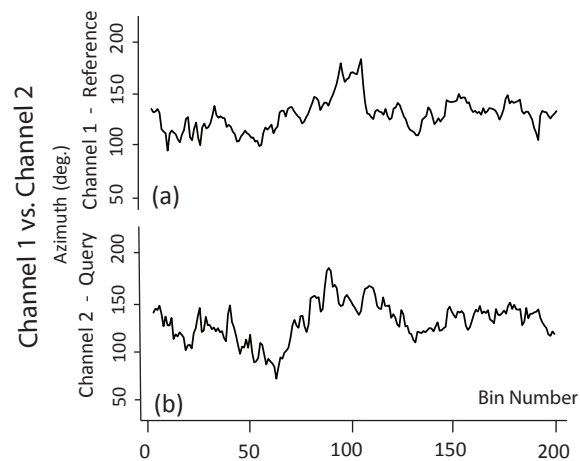
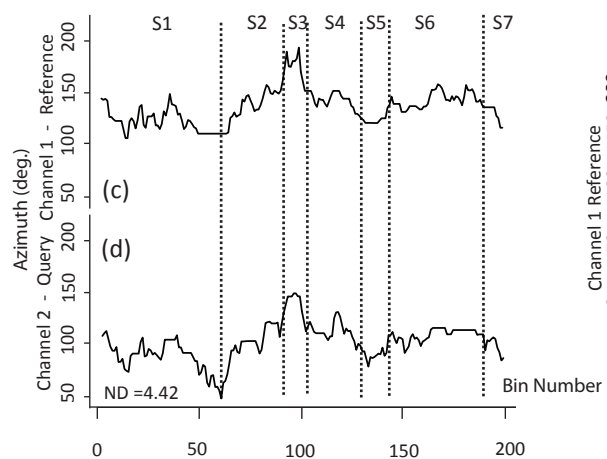


Figure 8.

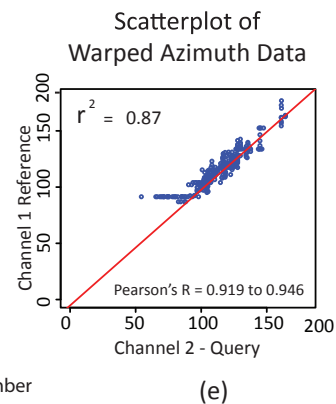
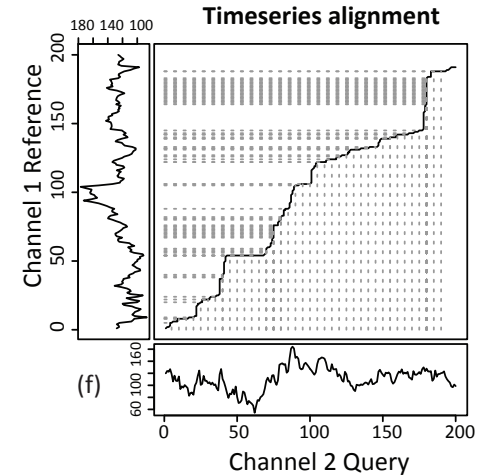
Initial Profiles



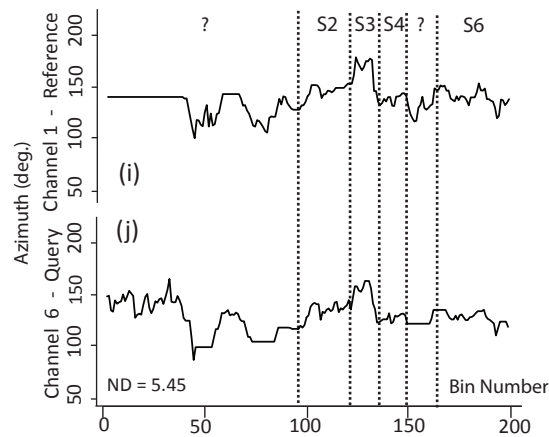
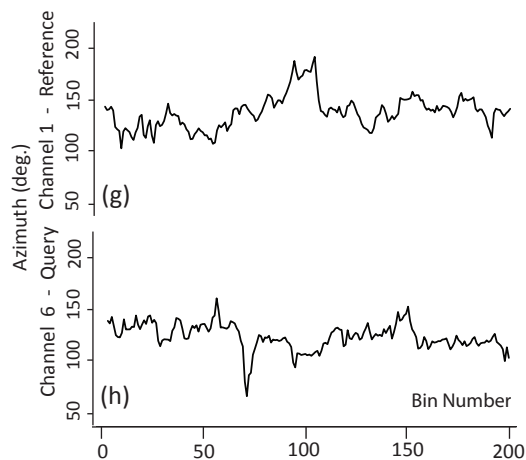
Post Warp Profiles and Channel Stages



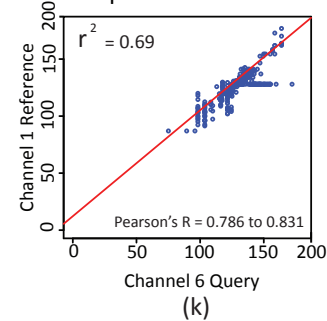
Post Warp Linear Regression

DTW
3 Way Plots
Timeseries alignment

Channel 1 vs. Channel 6



Scatterplot of Warped Azimuth Data



Timeseries alignment

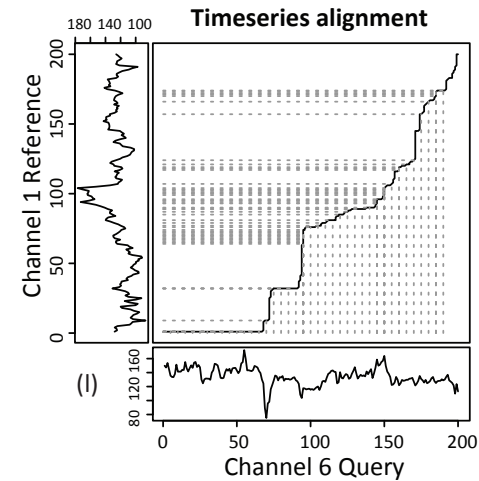
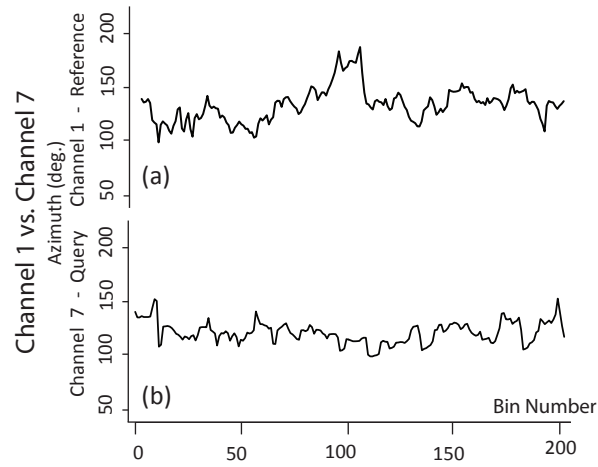
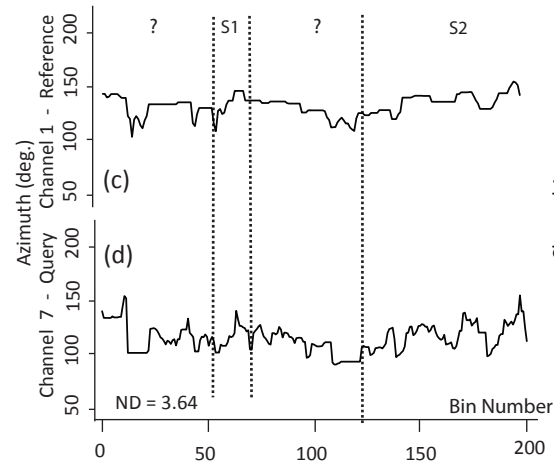


Figure 9.

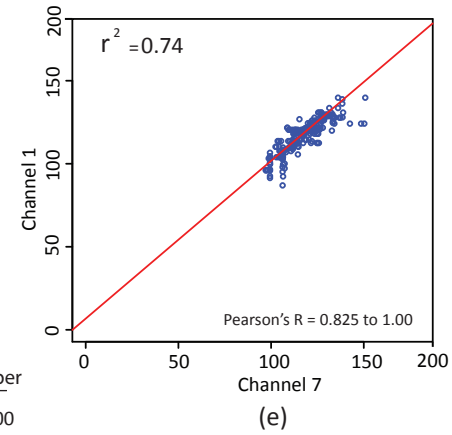
Initial Profiles



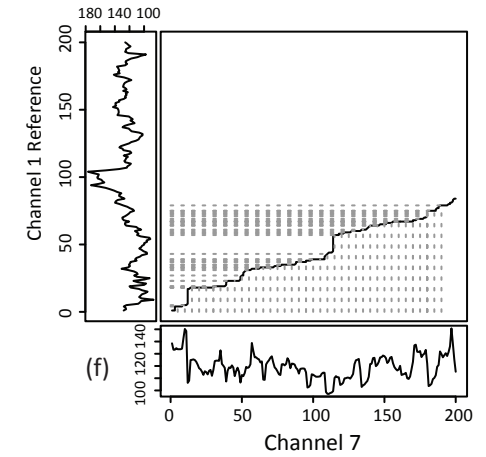
Post Warp Profiles and Channel Stages



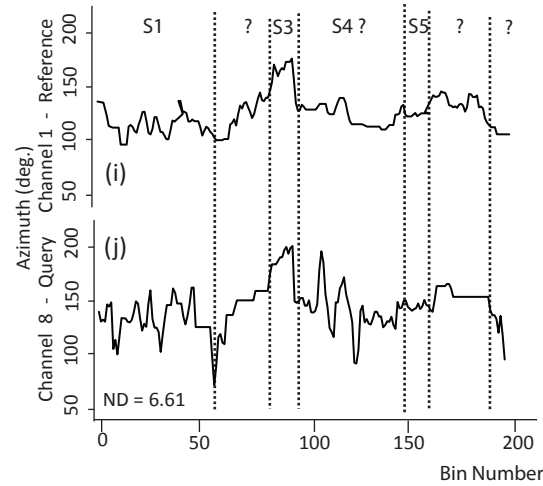
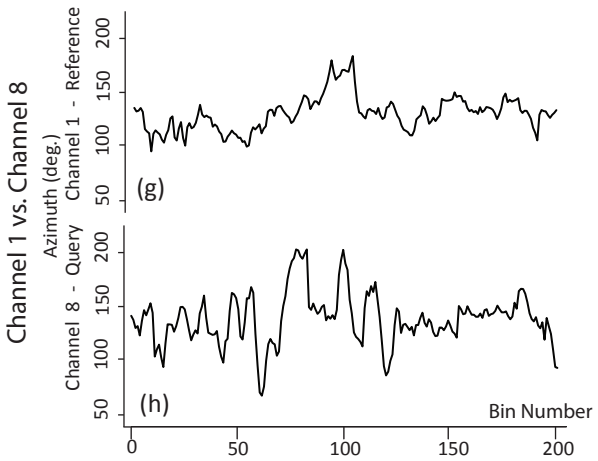
Post Warp Linear Regression Scatterplot of Warped Azimuth Data



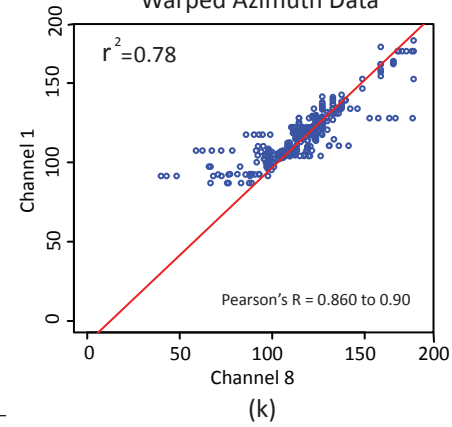
DTW 3 Way Plots Timeseries alignment



Channel 1 vs. Channel 8



Scatterplot of Warped Azimuth Data



DTW 3 Way Plots Timeseries alignment

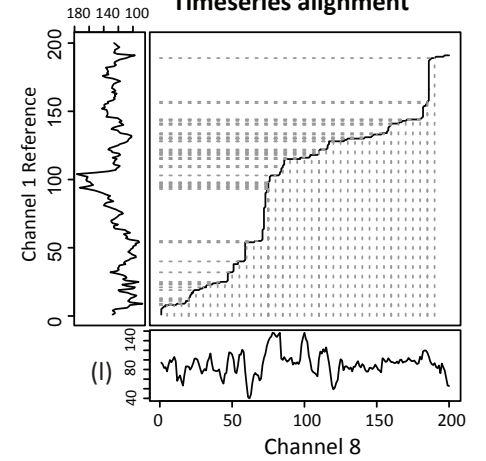
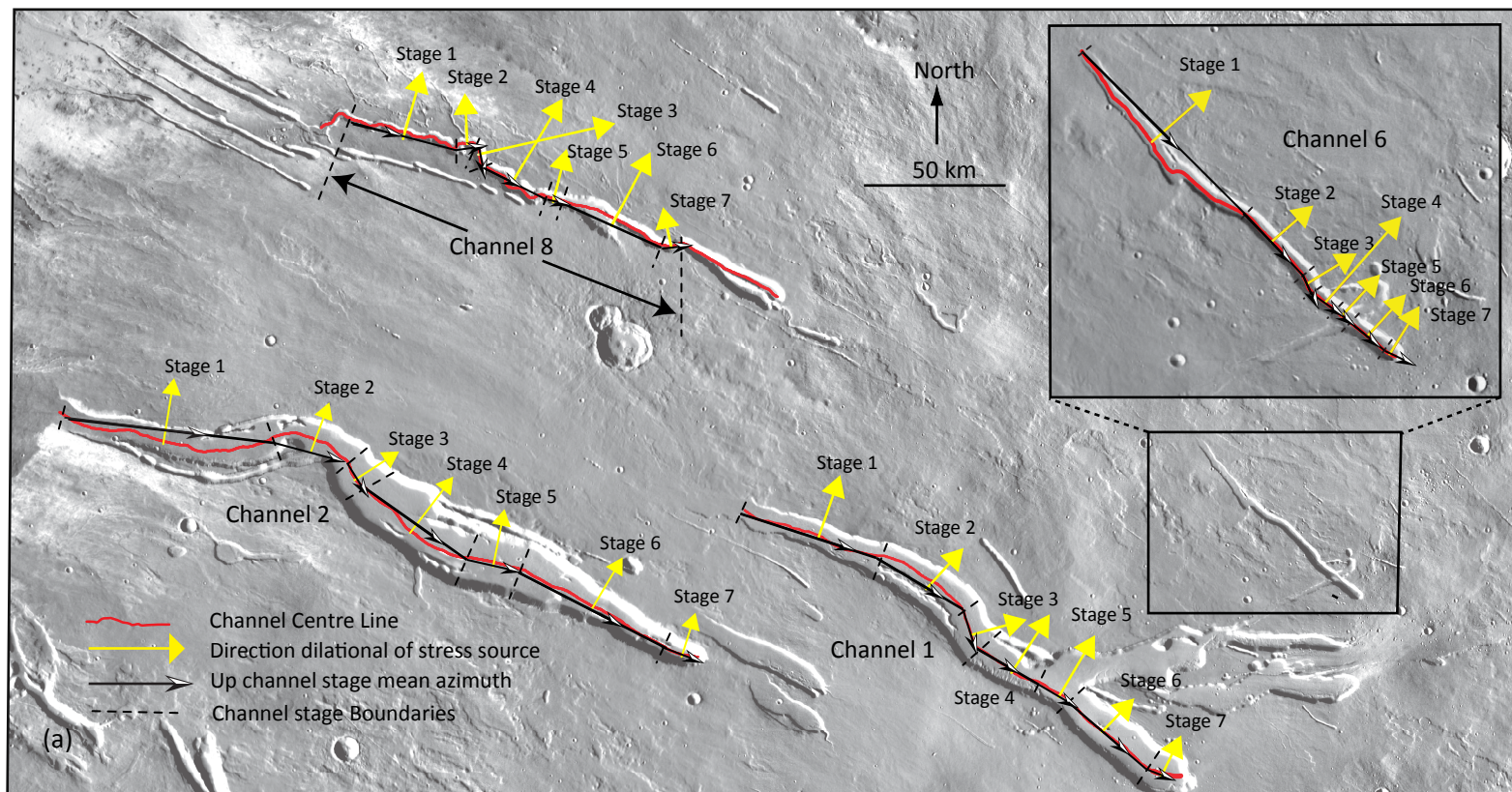
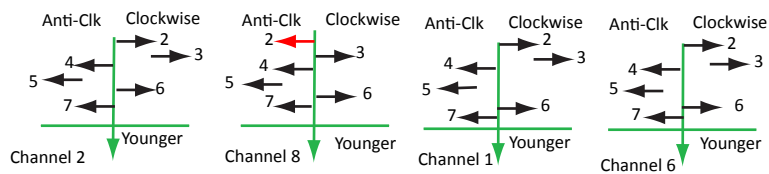


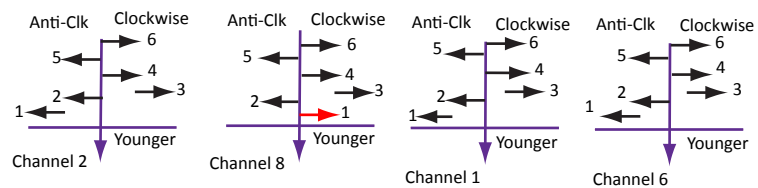
Figure 10.



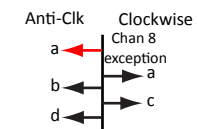
(b) Fault or gradient controlled channel migration headwards



(c) Fault or gradient controlled channel migration mouthwards



(d) Stress Direction Changes



(e) Stress Direction Changes

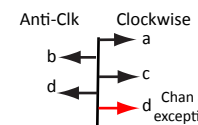
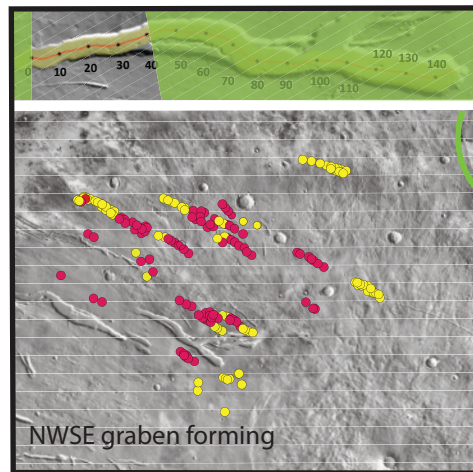
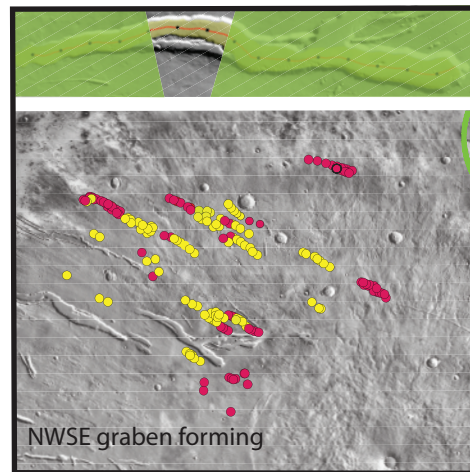


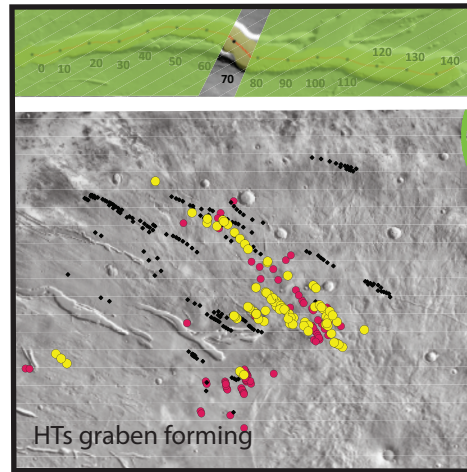
Figure 11.



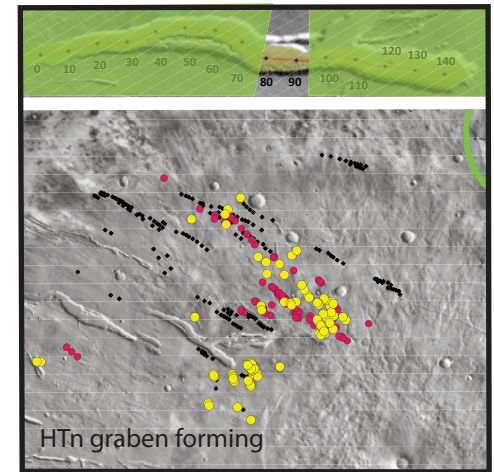
(a) Stage 1



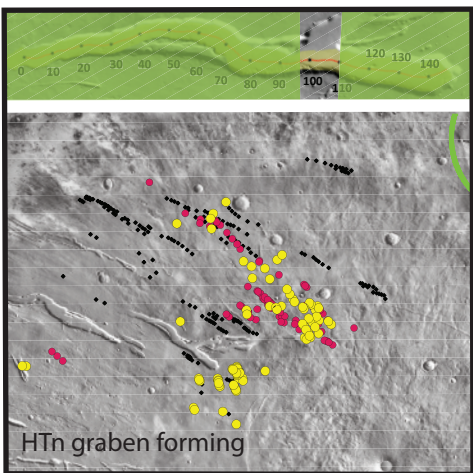
(b) Stage 2



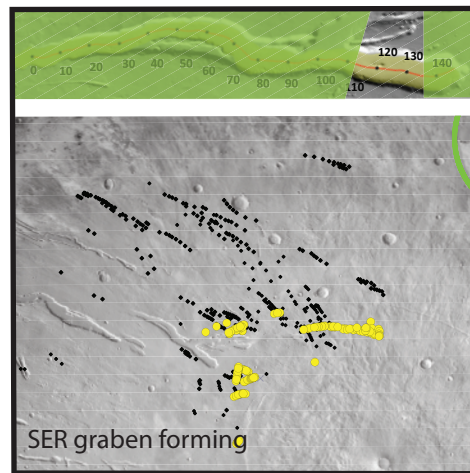
(c) Stage 3



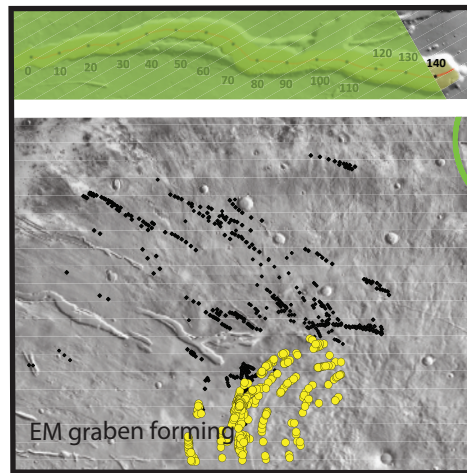
(d) Stage 4



(e) Stage 5



(f) Stage 6



(g) Stage 7

Key

- Graben forming in the window shown
- ◆ Graben already formed

The graben azimuth in Stages 1 and 2 cluster and also in Stages 3, 4 and 5 cluster are pointing towards their respective features. Within both of these clusters spatially associated groups are identified and the graben group not forming at the same time as the corresponding channel section are shown in red. ● Where there is little change in graben azimuth and hence in successive channel direction, e.g. Stage 4 and 5, it has not been possible to determine a meaningful spatial subdivision of that group